ELECTRONIC AND OPTICAL PROPERTIES OF AN ARTIFICIAL BENZENE RING

Milos Vladisavljevic

Thesis submitted to the Faculty of Graduate and Postdoctoral Studies in partial fulfillment of the requirements for the Master's degree in Physics

Department of Physics

Faculty of Science

University of Ottawa

Abstract

In this thesis, we develop the methodology for exploring the electronic and optical properties of an artificial benzene ring, both analytically as well as numerically through direct diagonalization using the configuration interaction method. We use the extended Hubbard Hamiltonian to model the interactions with different numbers of electrons, with spin projection and total spin resolved as good quantum numbers. The focus in this work is on the charged case and the emergence of an artificial gauge field and how it can be detected optically. We also examine three other cases of the artificial benzene ring, the single electron case, the charge neutral or half filled case, and the quarter filled case. Ground state properties, excited state spectra, and interactions with light are described.

Acknowledgments

I would like to thank Dr. Pawel Hawrylak, my research supervisor, for taking me on as his master's student and for always giving me the motivation for the work we were doing as well as the inspiration to do it. I would also like to thank Dr. Marek Korkusinski, and Isil Ozfidan for the constant help and support they have given me throughout my research. Without their assistance, as well as their previous work that I have built upon, I wouldn't understand a tenth of the work I have done over my master's thesis. Finally, I would like to thank my family and friends for putting up with me when I have tried to explain my research to them, and subsequently trying to use them as sound boards.

Contents

1 Introduction

There has been interest in creating artificial atoms at a mesoscopic scale[1,2]. This has been done through the creation of lateral quantum dots, where when a gate is added, electrons can be confined and controlled through electronic means. Single[3–5], double[6–11], triple[12–23] and quadruple[24–32] quantum dot structures have been extensively studied, both theoretically as well as experimentally. It is now possible to create artificial molecules with 6 quantum dots, an artificial benzene ring (ABR). This is interesting due to the ABR being the building block of graphene and graphite. An ABR can also be created as a ring within a semiconducting nanowire. All semiconducting nanowires have a hexagonal shape due to the crystalline structure citeBlmers, Albert, Poole. This topology, that of a ring configuration, can confine the electrons to the corners of the hexagon, thereby creating 6 1D electron gases which, with additional metallic gates, creates the quantum dots within the wire[36].

The benzene molecule[37–40] is made up of six carbon atoms in a planar hexagon formation, where each carbon atom is bonded to two neighboring carbons and a hydrogen atom (figure 1.). This bonding comes from the hybridization of the 2s, $2p_x$, and $2p_y$ orbitals into sp^2 hybrids which then form σ bonds with two other carbon atoms and one hydrogen atom. This leaves one unpaired electron in the $2p_z$ orbital. These unpaired electrons become delocalized and form six π bonds that are spread over the whole ring. These six delocalized electrons fill up the 3 lowest energy molecular orbitals, two in each, leaving the three remaining π orbitals empty.

An ABR is a two dimensional structure made of 6 quantum dots, each with orbitals equivalent of the $2p_z$ orbitals of the benzene molecule. The ABR is tunable through the variation of the separation of quantum dots, and the strength of electron-electron interactions, whereas the benzene molecule has set values. By increasing the scale of this structure, created with gated dots, or a nanowire, thus allowing the potentials to be controlled through either design of the structure or by adding electrodes in order to control it electronically after construction. The tuning of this structure can be accomplished by the changing of distances between dots, as well as changing their sizes, or through purely electronic means by attaching gates between the dots allowing for tunability after construction. Work has been done experimentally creating hexagonal nanowires (figure 2.) as well as lateral quantum dots and graphene-like structures[42].

In this thesis, we explore the electronic and optical properties of the ABR, both analytically as well as numerically through direct diagonalization. We use the extended Hubbard Hamiltonian to model the interactions between electrons. The focus in this work is on four main cases of the ABR with variable numbers of electrons, with the single electron case, the charge neutral or half filled case, the charged case, and the quarter filled case, considered in detail. Ground state properties, excited state spectra, and interaction with light are described.

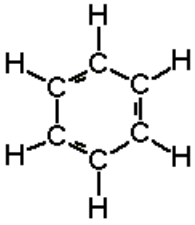

Figure 1: Representation of the benzene ring[41].

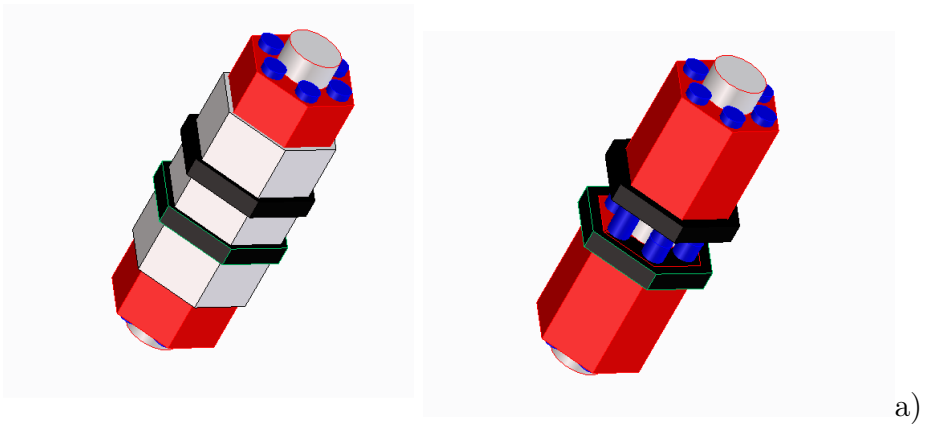

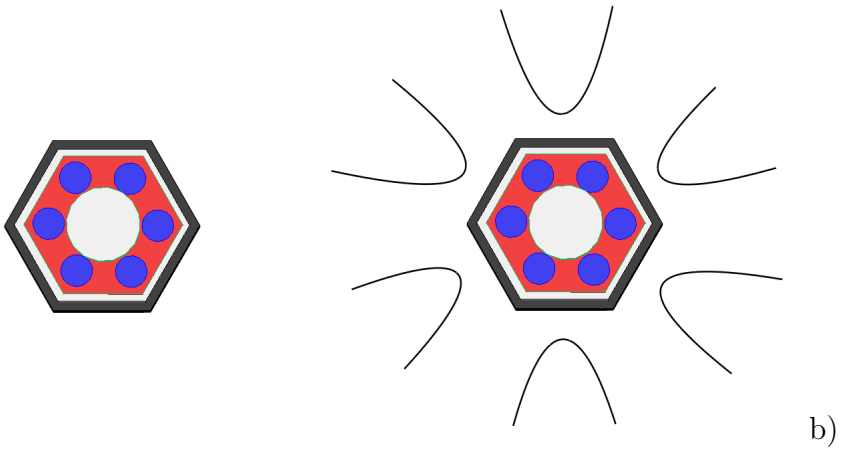

Figure 2: Representation of the artificial benzene ring construction, electron channels are marked blue, insulator material is marked white, conductive material is marked red, and electrodes are marked black, a) nanowire with and without outer layer, b) crosssection of wire without (left) and with (right) electrodes added to confine electrons to the corners of the hexagon.

2 The Model

2.1 The Extended Hubbard Hamiltonian

Electronic properties of an ABR are described in the extended Hubbard model with one spin degenerate orbital per dot[18,21,30]. In the Hubbard model, the Hamiltonian is characterized by the energy levels of the ith quantum dot E_i, the on-site Hubbard repulsion U_i, the tunneling element t_{ij} and direct Coulomb matrix elements V_{ij} between electron in dots i and j. The Hamiltonian in site representation is written as

$$\hat{H} = \sum_{\sigma,i=1}^{6} E_i c_{i\sigma}^{+} c_{i\sigma} - \sum_{\sigma\langle i,j\rangle}^{6} t_{ij} c_{i\sigma}^{+} c_{j\sigma} + \sum_{i=1}^{6} U_i n_{i\uparrow} n_{i\downarrow} + \frac{1}{2} \sum_{\langle i,j\rangle}^{6} V_{ij} \rho_i \rho_j, \tag{1}$$

where $c_{i\sigma}^{+}(c_{i\sigma})$ are operators creating (annihilating) an electron with spin σ on the orbital of the ith dot, $|i\rangle$. Here, $n_{i\sigma} = c_{i\sigma}^{+} c_{i\sigma}$ and $\rho_i = n_{i\downarrow} + n_{i\uparrow}$ are the number operator and charge density, respectively. We sum over the nearest-neighbor (NN) dots $\langle i, j\rangle$ for the interactions V_{ij}, and t_{ij}, between dots (figure 3.). There is a single energy level per dot, allowing up to $N_e = 12$ electrons to occupy the artificial benzene molecule. In an ABR it is possible to control and vary the electron density. In this work we look at the cases with $N_e = 1$ (the single particle case), $N_e = 3$ (the quarter filled case), $N_e = 5$ (charged ABR), and $N_e = 6$ (charge neutral case), with focus on the N=1 and N=5 cases.

To diagonalize the single particle Hamiltonian we express the Hamiltonian in Fourier space using the Fourier transformed creation/annihilation operators[30]

$$c_j^{+} = \frac{1}{\sqrt{6}} \sum_{\kappa_i} e^{-I\kappa_i j} b_{\kappa_i}^{+}\,, \tag{2}$$

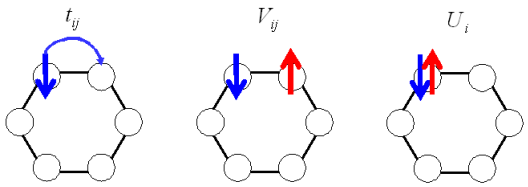

Figure 3: Graphical representation of electron interactions, where t_{ij}, V_{ij}, and U_i are the tunneling energy, electron-electron repulsion, and onsite repulsion, respectively.

where $b^+_{\kappa_i}$ creates an electron on a molecular orbital, and where the allowed wavevectors of the electron are $\kappa = \left\{0, \frac{\pi}{3}, -\frac{\pi}{3}, \frac{2\pi}{3}, -\frac{2\pi}{3}, \pi\right\}$. These are the wavevectors allowed due to the orthogonality of the creation (annihilation) operators. In this work the dots are assumed to be identical and on resonance, i.e., $E_i = E$, $U_i = U$, $V_{ij} = V$. Then using equation (2) in concert with equation (1), we can represent the Hamiltonian in Fourier space as[30],

$$\hat{H} = \sum_{\sigma,i} \epsilon_{\kappa_i} b^+_{\kappa_i\sigma} b_{\kappa_i\sigma} + \frac{1}{2} \sum_{ijkl,\sigma\sigma'} \langle \kappa_{i\sigma}\kappa_{j\sigma'}| \, V_{ee} \, |\kappa_{k\sigma'}\kappa_{l\sigma}\rangle \, b^+_{\kappa_{i\sigma}} b^+_{\kappa_{j\sigma'}} b_{\kappa_{k\sigma'}} b_{\kappa_{l\sigma}} \, . \tag{3}$$

Here V_{ee} is the electron-electron interaction, ϵ_{κ_i} is the energy of the molecular state, $\epsilon_{\kappa_i} = E - 2|t| \cos \kappa_i$[30]. This is the diagonalized single particle Hamiltonian. The Coulomb scattering term was obtained by solving separately for terms containing V and U.

$$H_V = \sum_{ijkl,\sigma\sigma'} \langle \kappa_{i\sigma}\kappa_{j\sigma'}| \, V_{ee} \, |\kappa_{k\sigma'}\kappa_{l\sigma}\rangle \, b^+_{\kappa_{i\sigma}} b^+_{\kappa_{j\sigma'}} b_{\kappa_{k\sigma'}} b_{\kappa_{l\sigma}} \tag{4}$$

$$= \sum_{<ij>,\sigma\sigma'} \langle \kappa_{i\sigma}\kappa_{j\sigma'}| \, V_{ee} \, |\kappa_{j\sigma'}\kappa_{i\sigma}\rangle \, b^+_{\kappa_{i\sigma}} b^+_{\kappa_{j\sigma'}} b_{\kappa_{k\sigma'}} b_{\kappa_{l\sigma}} \, . \tag{5}$$

$$H_V = \frac{1}{36}\sum_{<ij>}(\sum_{\kappa_i} e^{-I\kappa_i i} b^+_{\kappa_i} \sum_{\kappa_j} e^{-I\kappa_j j} b^+_{\kappa_j}) V (\sum_{\kappa_k} e^{I\kappa_k j} b_{\kappa_k} \sum_{\kappa_l} e^{I\kappa_l i} b_{\kappa_l}) \,, \tag{6}$$

$$H_V = \frac{V}{36}\sum_{\kappa_i}\sum_{\kappa_j}\sum_{\kappa_k}\sum_{\kappa_l}\left(\sum_{<ij>} e^{-I[(\kappa_i-\kappa_l)i+(\kappa_j-\kappa_k)j]}\right) b^+_{\kappa_i} b^+_{\kappa_j} b_{\kappa_k} b_{\kappa_l}. \tag{7}$$

Where we have V_{ee} equal to V. Since we are dealing with nearest neighbor interactions only, we have $j = i \pm 1$, and

$$H_V = \frac{V}{36}\sum_{\kappa_i}\sum_{\kappa_j}\sum_{\kappa_k}\sum_{\kappa_l}\left(\sum_i [e^{-I[(\kappa_i-\kappa_l+\kappa_j-\kappa_k)i+(\kappa_j-\kappa_k)]} + e^{-I[(\kappa_i-\kappa_l+\kappa_j-\kappa_k)i-(\kappa_j-\kappa_k)]}]\right) b^+_{\kappa_i} b^+_{\kappa_j} b_{\kappa_k} b_{\kappa_l}$$

$$H_V = \frac{V}{36}\sum_{\kappa_i}\sum_{\kappa_j}\sum_{\kappa_k}\sum_{\kappa_l}\left(\sum_i [e^{-I[(\kappa_i-\kappa_l+\kappa_j-\kappa_k)i}[e^{I(\kappa_j-\kappa_k)} + e^{-I(\kappa_j-\kappa_k)}]]\right) b^+_{\kappa_i} b^+_{\kappa_j} b_{\kappa_k} b_{\kappa_l}. \tag{8}$$

This is only nonzero for $(\kappa_i - \kappa_l + \kappa_j - \kappa_k) = 0$ which gives us our selection rules, $\delta(\kappa_i + \kappa_j - \kappa_k + \kappa_l)$.

$$H_V = \sum_{\kappa_i}\sum_{\kappa_j}\sum_{\kappa_k}\sum_{\kappa_l}\left(\frac{2V cos(\kappa_j - \kappa_k)}{6}\delta(\kappa_i + \kappa_j - \kappa_k + \kappa_l)\right) b^+_{\kappa_i} b^+_{\kappa_j} b_{\kappa_k} b_{\kappa_l} \,, \tag{9}$$

The on-site Hubbard repulsion energy is between two electrons of opposing spin on the same quantum dot, therefore the only position index we have is i.

$$H_U = \sum_{i,\sigma\sigma'} \langle \kappa_{i\sigma}\kappa_{i\sigma'}| V_{ee} |\kappa_{i\sigma'}\kappa_{i\sigma}\rangle \, b^+_{\kappa_{i\sigma}} b^+_{\kappa_{j\sigma'}} b_{\kappa_{k\sigma'}} b_{\kappa_{l\sigma}} \,,$$

$$H_U = \frac{U}{36}\sum_{\kappa_i}\sum_{\kappa_j}\sum_{\kappa_k}\sum_{\kappa_l}(\sum_i e^{-I[(\kappa_i-\kappa_l+\kappa_j-\kappa_k)i]}) b^+_{\kappa_i\uparrow} b^+_{\kappa_j\downarrow} b_{\kappa_k\downarrow} b_{\kappa_l\uparrow} \,, \tag{10}$$

where V_{ee} is equal to U in this case. This summation is only nonzero when $\kappa_i - \kappa_l + \kappa_j - \kappa_k = 0$, therefore:

$$H_U = \frac{U}{6}\sum_{\kappa_i}\sum_{\kappa_j}\sum_{\kappa_k}\sum_{\kappa_l}\delta\left(\kappa_i+\kappa_j-\kappa_k+\kappa_l\right)b^+_{\kappa_i\uparrow}b^+_{\kappa_j\downarrow}b_{\kappa_k\downarrow}b_{\kappa_l\uparrow}\,. \tag{11}$$

Therefore, putting the two interaction terms together gives us our Fourier transformed Coulomb interaction term,

$$\langle\kappa_i\kappa_j|\,V_{ee}\,|\kappa_k\kappa_l\rangle = \langle\kappa_i\kappa_j|\,H_V+H_U\,|\kappa_k\kappa_l\rangle\ , \tag{12}$$

$$\langle\kappa_i\kappa_j|\,V_{ee}\,|\kappa_k\kappa_l\rangle = \frac{U+2V\cos(\kappa_j-\kappa_k)}{6}\delta\left(\kappa_i+\kappa_j-\kappa_k+\kappa_l\right)\ . \tag{13}$$

In order to use this Hamiltonian in the configuration interaction method [43] we define the Coulomb interaction part of the Hamiltonian,

$$H_C = \frac{1}{2}\sum_{ijkl,\sigma\sigma'}\langle\kappa_{i\sigma}\kappa_{j\sigma'}|\,V_{ee}\,|\kappa_{k\sigma'}\kappa_{l\sigma}\rangle\,b^+_{\kappa_{i\sigma}}b^+_{\kappa_{j\sigma'}}b_{\kappa_{k\sigma'}}b_{\kappa_{l\sigma}}\,. \tag{14}$$

Next we split the sum into those with $k<l$ and $k>l$, this gives us two summations with a pair of constrained indices.

$$\begin{aligned} H_C = \frac{1}{2}\Bigg(&\sum_{ij,k<l,\sigma\sigma'}\langle\kappa_{i\sigma}\kappa_{j\sigma'}|\,V_{ee}\,|\kappa_{k\sigma'}\kappa_{l\sigma}\rangle\,b^+_{\kappa_{i\sigma}}b^+_{\kappa_{j\sigma'}}b_{\kappa_{k\sigma'}}b_{\kappa_{l\sigma}} \\ &+\sum_{ij,k>l,\sigma\sigma'}\langle\kappa_{i\sigma}\kappa_{j\sigma'}|\,V_{ee}\,|\kappa_{k\sigma'}\kappa_{l\sigma}\rangle\,b^+_{\kappa_{i\sigma}}b^+_{\kappa_{j\sigma'}}b_{\kappa_{k\sigma'}}b_{\kappa_{l\sigma}}\Bigg)\ . \end{aligned} \tag{15}$$

By exchanging the $k\sigma'$ and $l\sigma$ indices in the second term and following the same procedure for the $i\sigma$ and $j\sigma'$ indices, we can simplify this expression into a two term summation over two pairs of constrained indices,

$$\begin{aligned} H_C = \sum_{i>j,k<l,\sigma\sigma'}\ &\big(\langle\kappa_{i\sigma}\kappa_{j\sigma'}|\,V_{ee}\,|\kappa_{k\sigma'}\kappa_{l\sigma}\rangle \\ &-\ \langle\kappa_{i\sigma}\kappa_{j\sigma'}|V_{ee}\,|\kappa_{l\sigma}\kappa_{k\sigma'}\rangle\,\delta_{\sigma\sigma'}\big)\ \ b^+_{\kappa_{i\sigma}}b^+_{\kappa_{j\sigma'}}b_{\kappa_{k\sigma'}}b_{\kappa_{l\sigma}}\ , \end{aligned} \tag{16}$$

where we have now separated out the direct and exchange Coulomb interactions, the first and second term, respectively. The exchange energy is only active for

two electrons with the same spin, and the direct interaction is active between any two electrons regardless of spin. Putting the Coulomb interaction expression back into the original equation gives us the following Fourier transformed Hamiltonian suitable for numerical configuration interaction study:

$$\begin{aligned}\hat{H} = \sum_{\sigma,i} \epsilon_{\kappa_i} b^{+}_{\kappa_i \sigma} b_{\kappa_i \sigma} \quad &+ \quad \frac{1}{2} \sum_{i>j,k<l,\sigma\sigma'} (\langle \kappa_{i\sigma} \kappa_{j\sigma'} | \, V_{ee} \, | \kappa_{k\sigma'} \kappa_{l\sigma} \rangle \\ &- \quad \langle \kappa_{i\sigma} \kappa_{j\sigma'} | \, V_{ee} \, | \kappa_{l\sigma} \kappa_{k\sigma'} \rangle \, \delta_{\sigma\sigma'}) b^{+}_{\kappa_{i\sigma}} b^{+}_{\kappa_{j\sigma'}} b_{\kappa_{k\sigma'}} b_{\kappa_{l\sigma}} \, . \end{aligned} \tag{17}$$

We now have two Hamiltonians, one in site representation, suitable for strong electron-electron interactions, and one in molecular orbitals, suitable for weak electron-electron interactions.

2.2 Configuration Interaction Method

To solve for the electronic structure we create Hamiltonians in the space of electronic configurations. We distribute N electrons on either lattice sites, or molecular orbitals, and create all possible configurations. These configurations are characterized by their spin projections, S_z, and for molecular states by the configuration's total angular momentum, which is calculated by adding the individual angular momenta of the electrons, which are conserved and allow us to block diagonalize our Hamiltonian. The non-interacting energies for each configuration consist of the kinetic energy of all the electrons on the different energy levels. These terms we have on the diagonal of our Hamiltonian matrix. In addition, we add interaction energy of electrons in a given configuration. We then introduce all of the Coulomb scattering interactions between the configurations, which couple one configuration to another. To do this we use equations (12) and (17), which

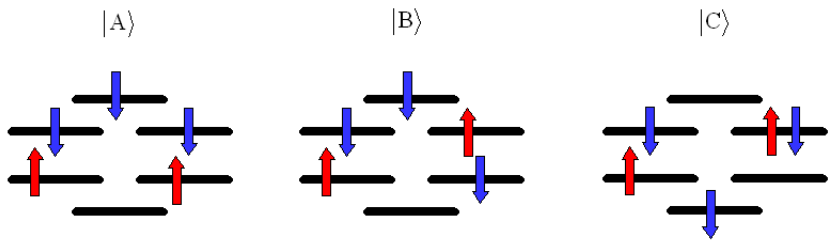

Figure 4: Example configurations A, B, and C for configuration interaction method. We use bars to describe our molecular orbitals with increasing energy, as opposed to using the hexagonal diagram with shown sites for our atomic orbitals.

allowed us to create our complete Hamiltonian matrix.

For example, we consider three five-electron configurations shown in figure 4, with the convention that the lowest numbered molecular orbital goes to the left most position and gets higher the farther right you go while keeping the spin-up electrons together at the front: $|A\rangle = |b^+_{2_\uparrow} b^+_{3_\uparrow}\rangle |b^+_{4_\downarrow} b^+_{5_\downarrow} b^+_{6_\downarrow}\rangle$, $|B\rangle = |b^+_{2_\uparrow} b^+_{5_\uparrow}\rangle |b^+_{3_\downarrow} b^+_{4_\downarrow} b^+_{6_\downarrow}\rangle$, and $|C\rangle = |b^+_{2_\uparrow} b^+_{5_\uparrow}\rangle |b^+_{1_\downarrow} b^+_{4_\downarrow} b^+_{5_\downarrow}\rangle$, where configuration B is just A but with the electrons 5 and 3 exchanging spins, and configuration C is just B but with two down spins moved, one to allow us to look at double occupation of molecular levels, and the other one to adjust for total angular momentum. For the diagonal components of our matrix we have the first and second terms in equation (17). In molecular basis we solve for the kinetic energy and Coulomb interaction by looking at how

the configuration interacts with itself:

$$\begin{aligned}
\langle A|\sum_{\sigma,i}\epsilon_{\kappa_i}b^+_{\kappa_i\sigma}b_{\kappa_i\sigma}|A\rangle &= \langle b_{6_\downarrow}b_{5_\downarrow}b_{4_\downarrow}b_{3_\uparrow}b_{2_\uparrow}|\sum_{\sigma,i}\epsilon_{\kappa_i}b^+_{\kappa_i\sigma}b_{\kappa_i\sigma}|b^+_{2_\uparrow}b^+_{3_\uparrow}b^+_{4_\downarrow}b^+_{5_\downarrow}b^+_{6_\downarrow}\rangle\,, \\
\langle A|\sum_{\sigma,i}\epsilon_{\kappa_i}b^+_{\kappa_i\sigma}b_{\kappa_i\sigma}|A\rangle &= -2|t|\Big(cos(\kappa_{b^+_{2_\uparrow}})+cos(\kappa_{b^+_{3_\uparrow}}) \\
&+ cos(\kappa_{b^+_{4_\downarrow}})+cos(\kappa_{b^+_{5_\downarrow}})+cos(\kappa_{b^+_{6_\downarrow}})\Big)\,, \qquad (18)
\end{aligned}$$

Where $\kappa_{b^+_{2\downarrow}}=-\pi/3$, $\kappa_{b^+_{3\uparrow}}=\pi/3$, $\kappa_{b^+_{4\downarrow}}=2\pi/3$, $\kappa_{b^+_{5\downarrow}}=-2\pi/3$, and $\kappa_{b^+_{6\downarrow}}=\pi$.

$$\langle A|\sum_{\sigma,i}\epsilon_{\kappa_i}b^+_{\kappa_i\sigma}b_{\kappa_i\sigma}|A\rangle = +2t\,. \qquad (19)$$

This is our non-interacting energy for configuration $|A\rangle$. Now we look at the electron-electron interactions within the configuration.

$$\langle A|\sum_{i>j,k<l,\sigma\sigma'}\Big(\langle\kappa_{i\sigma}\kappa_{j\sigma'}|V_{ee}\,|\kappa_{k\sigma'}\kappa_{l\sigma}\rangle-\langle\kappa_{i\sigma}\kappa_{j\sigma'}|\,V_{ee}\,|\kappa_{l\sigma}\kappa_{k\sigma'}\rangle\,\delta_{\sigma\sigma'}\Big) b^+_{\kappa_{i\sigma}}b^+_{\kappa_{j\sigma'}}b_{\kappa_{k\sigma'}}b_{\kappa_{l\sigma}}|A\rangle\,, \qquad (20)$$

$$\langle b_{6_\downarrow}b_{5_\downarrow}b_{4_\downarrow}b_{3_\uparrow}b_{2_\uparrow}|\sum_{i>j,k<l,\sigma\sigma'}\Big(\langle\kappa_{i\sigma}\kappa_{j\sigma'}V_{ee}\,|\kappa_{k\sigma'}\kappa_{l\sigma}\rangle-\langle\kappa_{i\sigma}\kappa_{j\sigma'}|\,V_{ee}\,|\kappa_{l\sigma}\kappa_{k\sigma'}\rangle\,\delta_{\sigma\sigma'}\Big)$$

$$b^+_{\kappa_{i\sigma}}b^+_{\kappa_{j\sigma'}}b_{\kappa_{k\sigma'}}b_{\kappa_{l\sigma}}|b^+_{2_\uparrow}b^+_{3_\uparrow}b^+_{4_\downarrow}b^+_{5_\downarrow}b^+_{6_\downarrow}\rangle\,. \qquad (21)$$

After summing over all indices that give nonzero values, we are left with:

$$\langle A|\sum_{i>j,k<l,\sigma\sigma'}\Big(\langle\kappa_{i\sigma}\kappa_{j\sigma'}V_{ee}\,|\kappa_{k\sigma'}\kappa_{l\sigma}\rangle-\langle\kappa_{i\sigma}\kappa_{j\sigma'}|\,V_{ee}\,|\kappa_{l\sigma}\kappa_{k\sigma'}\rangle\,\delta_{\sigma\sigma'}\Big)$$

$$b^+_{\kappa_{i\sigma}}b^+_{\kappa_{j\sigma'}}b_{\kappa_{k\sigma'}}b_{\kappa_{l\sigma}}|A\rangle = U+\frac{10V}{3}\,. \qquad (22)$$

Therefore our diagonal matrix element for configuration $|A\rangle$ is $2t + U + \frac{10V}{3}$. We perform similar calculations for our $|B\rangle$ and $|C\rangle$ configurations. This leaves us with a 3x3 matrix, in the space of A, B, and C configurations, with configuration interactions on the off diagonal to be determined,

$$H = \begin{bmatrix} 2t + U + \frac{10V}{3} & V_{AB} & V_{AC} \\ V_{BA} & 2t + U + 3V & V_{BC} \\ V_{CA} & V_{CB} & 2t + U + \frac{11V}{3} \end{bmatrix} .$$

To solve for these off diagonal elements, we follow the same process as for the diagonal elements. The kinetic energy goes to zero. Comparing $|A\rangle$ and $|B\rangle$, we compute the interaction energy,

$$\begin{aligned} V_{AB} &= \langle b_{6_\downarrow} b_{5_\downarrow} b_{4_\downarrow} b_{3_\uparrow} b_{2_\uparrow}| \sum_{i>j,k<l,\sigma\sigma'} (\langle \kappa_{i\sigma}\kappa_{j\sigma'}| V_{ee} |\kappa_{k\sigma'}\kappa_{l\sigma}\rangle \\ &- \langle \kappa_{i\sigma}\kappa_{j\sigma'}| V_{ee} |\kappa_{l\sigma}\kappa_{k\sigma'}\rangle \delta_{\sigma\sigma'}) b^+_{\kappa_{i\sigma}} b^+_{\kappa_{j\sigma'}} b_{\kappa_{k\sigma'}} b_{\kappa_{l\sigma}} |b^+_{2_\uparrow} b^+_{5_\uparrow} b^+_{3_\downarrow} b^+_{4_\downarrow} b^+_{6_\downarrow}\rangle , \end{aligned} \tag{23}$$

$$\begin{aligned} V_{AB} = \langle b_{6_\downarrow} b_{5_\downarrow} b_{4_\downarrow} b_{3_\uparrow} b_{2_\uparrow}| \sum_{i>j,k<l,\sigma\sigma'} (\langle \kappa_{i\sigma}\kappa_{j\sigma'}| V_{ee} |\kappa_{k\sigma'}\kappa_{l\sigma}\rangle) b^+_{\kappa_{i\sigma}} b^+_{\kappa_{j\sigma'}} b_{\kappa_{k\sigma'}} b_{\kappa_{l\sigma}} \\ |b^+_{2_\uparrow} b^+_{5_\uparrow} b^+_{3_\downarrow} b^+_{4_\downarrow} b^+_{6_\downarrow}\rangle , \end{aligned} \tag{24}$$

$$V_{AB} = \langle b_{5_\downarrow} b_{3_\uparrow}| \sum_{i>j,k<l,\sigma\sigma'} (\langle \kappa_{i\sigma}\kappa_{j\sigma'}| V_{ee} |\kappa_{k\sigma'}\kappa_{l\sigma}\rangle) b^+_{\kappa_{i\sigma}} b^+_{\kappa_{j\sigma'}} b_{\kappa_{k\sigma'}} b_{\kappa_{l\sigma}} |b^+_{5_\uparrow} b^+_{3_\downarrow}\rangle , \tag{25}$$

$$V_{AB} = \langle b_{5_\downarrow} b_{3_\uparrow}| (\langle \kappa_{3\uparrow}\kappa_{5\downarrow}| V_{ee} |\kappa_{3\downarrow}\kappa_{5\uparrow}\rangle) b^+_{\kappa_{3\uparrow}} b^+_{\kappa_{5\downarrow}} b_{\kappa_{3\downarrow}} b_{\kappa_{5\uparrow}} |b^+_{5_\uparrow} b^+_{3_\downarrow}\rangle , \tag{26}$$

$$V_{AB} = \frac{U + 2V\cos(\kappa_{5\downarrow} - \kappa_{3\downarrow})}{6} \delta\left(\kappa_{3\uparrow} + \kappa_{5\downarrow} - \kappa_{3\downarrow} + \kappa_{5\uparrow}\right) , \tag{27}$$

$$V_{AB} = \frac{U + 2V\cos(\frac{-2\pi}{3} - \frac{\pi}{3})}{6} \delta\left(\kappa_{3\uparrow} + \kappa_{5\downarrow} - \kappa_{3\downarrow} + \kappa_{5\uparrow}\right) , \tag{28}$$

$$V_{AB} = \frac{U - 2V}{6} \delta\left(\kappa_{3\uparrow} + \kappa_{5\downarrow} - \kappa_{3\downarrow} + \kappa_{5\uparrow}\right) . \tag{29}$$

Doing these calculations for V_{AC} and V_{BC} as well fills up our matrix:

$$H = \begin{bmatrix} 2t + U + \frac{10V}{3} & \frac{U-2V}{6} & \frac{U-2V}{6} \\ \frac{U-2V}{6} & 2t + U + 3V & \frac{V}{2} \\ \frac{U-2V}{6} & \frac{V}{2} & 2t + U + \frac{11V}{3} \end{bmatrix}.$$

This method allows us to create the Hamiltonian matrix for all configurations and, diagonalizing, obtain the eigenenergies and eigenstates we are looking for.

3 Electronic Structure of the Artificial Benzene Ring

3.1 One Electron Case

To begin looking at the ABR, we look at the simplest case available to us, that of the one electron. This case, discussed already, only has tunneling energy components and onsite energy, which leaves us with only the first two terms in equation (1), or in the Fourier basis described by equation (17), only the first term. The basis consists of six orthogonal states $\{|1\rangle, |2\rangle, |3\rangle, |4\rangle, |5\rangle, |6\rangle\}$, where $|i\rangle = c_i^+ |0\rangle$ which represents the creation of an electron on dot i. The diagonal elements of the Hamiltonian are the onsite energies of the dot, $\left\langle i \left| \hat{H} \right| i \right\rangle = E_i$, in this model we take this energy as zero. The off diagonal elements correspond to the tunneling of the electron from one dot to its nearest neighbor, $\left\langle j \left| \hat{H} \right| i \right\rangle = -t_{ij}$. The one electron moving through the ring gives us the following Hamiltonian matrix:

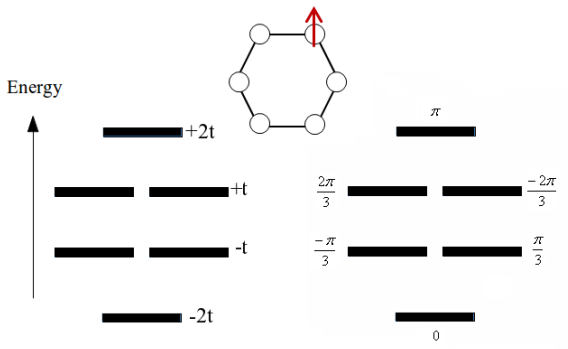

Figure 5: Representation of the artificial benzene ring as well as the single particle energy levels of the artificial benzene ring, showing both the energies of the levels (left) as well as the angular momentum of the individual levels (right).

$$H_{1e} = \begin{bmatrix} 0 & -t & 0 & 0 & 0 & -t \\ -t & 0 & -t & 0 & 0 & 0 \\ 0 & -t & 0 & -t & 0 & 0 \\ 0 & 0 & -t & 0 & -t & 0 \\ 0 & 0 & 0 & -t & 0 & -t \\ -t & 0 & 0 & 0 & -t & 0 \end{bmatrix}.$$

This matrix was diagonalized using equation (2), which rotates the matrix from site representation to molecular orbitals, which diagonalizes the single particle Hamiltonian. This gives us the eigenenergies $\{-2t, -t, -t, +t, +t, +2t\}$, how these energies relate to their corresponding wavevector can be seen in figure 5, and directly as $\epsilon_{\kappa_i} = E - 2|t| \cos \kappa_i$, where $\kappa = 0, \pm\pi/3, \pm 2\pi/3, \pi$, respectively for the eigenenergies.

3.2 Charge Neutral Case (Six Electrons)

Next we move to the charge neutral case with six electrons on the ABR. We call the six electron case charge neutral, this is because in the real benzene ring six carbon atoms and six electrons create a charge neutral molecule, and five electrons make it charged. Therefore we define the charge neutral case for our system as one electron per site. We begin this case by using the same technique described in section 2.2. We use the Fourier transformed equation (17) to look at finite U and V interactions for all configurations of the six electrons, i.e. S_z=3,2,1,and 0 which correspond to the spin polarized, one, two, and three minority spins, respectively. We then resolve total spin using our numerical code by separating the total spin states from the spin projection configurations, which requires the calculation of the interactions between configurations of sizes 1, 36, 225, and 400 for S_z=3,2,1,and 0 respectively. To get a sense of how the ground state energies of the different total spin states are affected by Coulomb interactions, we plot them in figure 6 as a function of U/t and V/t. We normalize both U and V to the tunneling energy t, because t is the smallest change in molecular orbital energy. We see that the ordering of the total spin ground states stays the same over changing U/t and V/t. The ground state, for 6 electrons, stays as the $S = 0$ state, then the first excited state is the $S = 1$, then $S = 2$, and finally the spin polarized $S = 3$ state. The chosen starting value for U/t is in keeping with U being greater than V to keep this in the realistic regime. Whereas the chosen ending point for V/t is when it becomes equal with the fixed U. For example, for a U = 5, V/t has a maximum of 5.

For $U \gg t$ we have a situation where each dot is only singly occupied in order to achieve the lowest total energy of the system. The interaction energy determines the charge distribution of the system. Therefore the only degree of freedom is the spin distribution of the system. However, if we consider the kinetic energy as a perturbation, we see that if electrons can have the option to tunnel to neighboring dots we have a virtual delocalization, where electrons are allowed to double occupy for infinitesimally small durations before exchanging dot positions, which reduces the kinetic energy and we have an effective interaction that favors neighboring electrons to have opposite spins. This makes our Hubbard model very similar to the Heisenberg model, equation (30), where only single occupation is allowed and the spins have lowest energy when they are anti parallel in orientation:

$$H = J\sum_{j=1}^{N}\sigma_j\sigma_{j+1} - h\sum_{j=1}^{N}\sigma_j \ , \tag{30}$$

where J is the coupling constant, h is an external magnetic field, and σ_j tracks the spin of an electron while σ_{j+1} tracks the spin of its neighbor. This is an interesting case due to its focus on the lower energy levels only, specifically the first Hubbard band. For calculations interested only in single occupation, the Heisenberg model provides a simplified expression to the Hubbard Hamiltonian.

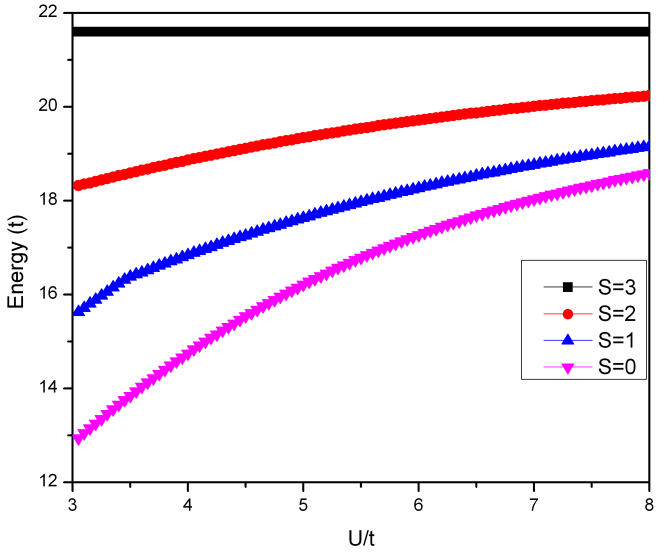

a)

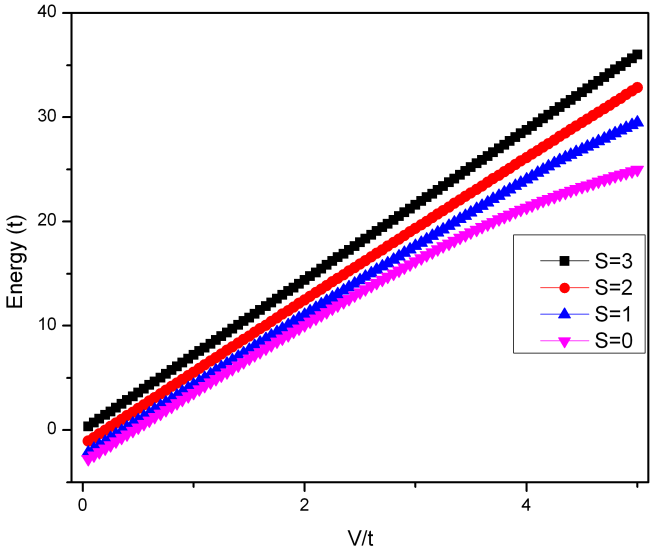

b)

Figure 6: Six electron case: a) Graph of ground state energy versus change of U/t with $V/t = 3$. b) Graph of ground state energy versus change of V/t with $U/t = 5$

3.3 Charged Case (Five Electrons)

3.3.1 Analytical Solution for the $U = \infty$ Case

To get an initial understanding of five electrons moving and interacting on six quantum dots, we call this the charged case since a benzene ring made of carbon atoms with five or seven electrons would be charged. We look at a simplified case of very strong interactions, with $U = \infty$, where double occupation is not allowed. We will work here in site representation. For five electrons there are three spin projections, $S_z = \frac{5}{2}$ with 6 configurations, $S_z = \frac{3}{2}$ with 30 configurations, and $S_z = \frac{1}{2}$ with 60 configurations.

A. $S_z = 5/2$ **Case**

We start by defining the ground state (GS) of a spin polarized C6 molecule,

$$|GS\rangle = \prod_{i=1}^{6} c_{i\downarrow}^{+} |0\rangle \ . \tag{31}$$

Then we define the five electron system by removing one electron from the C6 molecule's ground state, thus creating a quasi hole,

$$|n_h\rangle = c_{n_h\downarrow} |GS\rangle \ . \tag{32}$$

This gives us our spin polarized $S_z = \frac{5}{2}$ system. Comparing different hole positions allows us to create our Hamiltonian matrix, with $U = \infty$, $E = 0$, and $V = 0$, it

reads:

$$H = \begin{bmatrix} 0 & +t & 0 & 0 & 0 & +t \\ +t & 0 & +t & 0 & 0 & 0 \\ 0 & +t & 0 & +t & 0 & 0 \\ 0 & 0 & +t & 0 & +t & 0 \\ 0 & 0 & 0 & +t & 0 & +t \\ +t & 0 & 0 & 0 & +t & 0 \end{bmatrix} .$$

This is the matrix of the single electron Hamiltonian, however, since we are tracking a hole instead of an electron, we have positive tunneling elements instead of negative. This is due to the method we used to construct the five electron system, where we have a negative factor on every even numbered hole position, which results from equation (32).

B. $S_z = 3/2$ **Case**

To create the $S_z = \frac{3}{2}$ configurations we flip the spin of one of the electrons by using the annihilation operator to destroy a spin-down electron and a creation operator to create a spin-up electron.

$$|n_{h,j}\rangle = c^{+}_{j\uparrow} c_{j\downarrow} |n_h\rangle \ . \tag{33}$$

We then create an orthogonal basis of states for a given hole at n_h dressed with the quantum number κ to track the minority spin j. To keep our phases consistent and our states orthogonal we, in our summation, look at the electrons on the dots before the one with the hole and then at the ones after[30].

$$|\kappa, n_{h,j}\rangle = \sum_{j=0, j<n_h}^{5} e^{I\kappa j} |j\rangle + \sum_{j=0, j>n_h}^{5} e^{I\kappa(j-1)} |j\rangle \ , \ \kappa = \frac{2\pi}{5} n, \ n = 0, 1, ..., 4 \ . \tag{34}$$

Using this condition and method of writing out the state of the system, we look at different positions of the hole on the dots which takes our 30 states and gives us 6 states made up of a linear combination of 5 configurations , and we have the resulting 6x6 Hamiltonian matrix for each spin state κ:

$$H = \begin{bmatrix} 0 & +t & 0 & 0 & 0 & +te^{-I\kappa} \\ +t & 0 & +t & 0 & 0 & 0 \\ 0 & +t & 0 & +t & 0 & 0 \\ 0 & 0 & +t & 0 & +t & 0 \\ 0 & 0 & 0 & +t & 0 & +t \\ +te^{+I\kappa} & 0 & 0 & 0 & +t & 0 \end{bmatrix} . \tag{35}$$

We see that this matrix is similar to the the spin polarized case, except for positive tunneling values, as well as these added phase factors when tunneling between quantum dots one and six. These added phase factors act as if there is a magnetic field threading through the ring, we call this an artificial gauge field, which defines how different values of κ affect the eigenenergies, since without these phase factors we would have a 5 fold degenerate system. To diagonalize this Hamiltonian, equation (35), we create the following eigenfunctions:

$$|Q;\kappa\rangle = \sum_{n_h=1}^{6} e^{IQn_h} e^{I\phi n_h} |\kappa, n_{h,j}\rangle \ . \tag{36}$$

Diagonalizing the Hamiltonian with these eigenfunctions, we have that the added factor ϕ tracks the phase accumulated by the hole from every tunneling event across the ring, leading to $\phi = \frac{\kappa}{6}$. Solving for Q using the condition of orthogonality, results in $Q = \frac{2\pi}{6}n$, where $n = 0, 1..., 5$. This leads to eigenvalues of the form

(figure 7.):

$$E_{Q,\kappa} = -2t\cos(Q + \frac{\kappa}{6})\,, \tag{37}$$

where $\kappa = \frac{2\pi}{5}m$, $m = 0, 1..., 4$. Now we have a new wavevector, G, made up of two independent variables Q and κ: $G = Q + \frac{\kappa}{6}$. In figure 7a we plot the allowed eigenenergies as a function of this wavevector G.

C. $S_z = 1/2$ **Case**

For the $S_z = \frac{1}{2}$ case we take a slightly different approach in defining the basis, this method is based on the Caspers and Iske method[44] using their cyclic permutation operator $\hat{\mathrm{P}}$.

$$\hat{\mathrm{P}} : \{\sigma_1, \sigma_2, ..., \sigma_n\} \rightarrow \{\sigma_n, \sigma_1, ..., \sigma_{n-1}\}$$

This operator shuffles all of the electrons to the right, while ignoring the hole position. This allows us to recreate the whole Hilbert space by creating unique subspaces that do not interact with each other. Using this operator we can define two separate subspaces, one where the two up electrons travel together, $\uparrow\uparrow$, as they are permuted around the benzene ring, and one where a grouping of three electrons in the configuration $\uparrow\downarrow\uparrow$ moves through the system together (figure 8.).

$$\begin{aligned}
|\mathrm{A}_1\rangle &= |\mathrm{c}^+_{2_\uparrow} c^+_{3_\uparrow} c^+_{4_\downarrow} c^+_{5_\downarrow} c^+_{6_\downarrow}\rangle\,, & |A'_1\rangle &= |\mathrm{c}^+_{2_\uparrow} c^+_{3_\downarrow} c^+_{4_\uparrow} c^+_{5_\downarrow} c^+_{6_\downarrow}\rangle\,, \\
\hat{\mathrm{P}}|\mathrm{A}_1\rangle = |A_2\rangle &= |\mathrm{c}^+_{2_\downarrow} c^+_{3_\uparrow} c^+_{4_\uparrow} c^+_{5_\downarrow} c^+_{6_\downarrow}\rangle\,, & \hat{\mathrm{P}}|A'_1\rangle = |A'_2\rangle &= |\mathrm{c}^+_{2_\downarrow} c^+_{3_\uparrow} c^+_{4_\downarrow} c^+_{5_\uparrow} c^+_{6_\downarrow}\rangle\,, \\
\hat{\mathrm{P}}|\mathrm{A}_2\rangle = |A_3\rangle &= |\mathrm{c}^+_{2_\downarrow} c^+_{3_\downarrow} c^+_{4_\uparrow} c^+_{5_\uparrow} c^+_{6_\downarrow}\rangle\,, & \hat{\mathrm{P}}|A'_2\rangle = |A'_3\rangle &= |\mathrm{c}^+_{2_\downarrow} c^+_{3_\downarrow} c^+_{4_\uparrow} c^+_{5_\downarrow} c^+_{6_\uparrow}\rangle\,, \\
\hat{\mathrm{P}}|\mathrm{A}_3\rangle = |A_4\rangle &= |\mathrm{c}^+_{2_\downarrow} c^+_{3_\downarrow} c^+_{4_\downarrow} c^+_{5_\uparrow} c^+_{6_\uparrow}\rangle\,, & \hat{\mathrm{P}}|A'_3\rangle = |A'_4\rangle &= |\mathrm{c}^+_{2_\uparrow} c^+_{3_\downarrow} c^+_{4_\downarrow} c^+_{5_\uparrow} c^+_{6_\downarrow}\rangle\,, \\
\hat{\mathrm{P}}|\mathrm{A}_4\rangle = |A_5\rangle &= |\mathrm{c}^+_{2_\uparrow} c^+_{3_\downarrow} c^+_{4_\downarrow} c^+_{5_\downarrow} c^+_{6_\uparrow}\rangle\,, & \hat{\mathrm{P}}|A'_4\rangle = |A'_5\rangle &= |\mathrm{c}^+_{2_\downarrow} c^+_{3_\uparrow} c^+_{4_\downarrow} c^+_{5_\downarrow} c^+_{6_\uparrow}\rangle\,, \\
\hat{\mathrm{P}}|\mathrm{A}_5\rangle = |A_1\rangle &= |\mathrm{c}^+_{2_\uparrow} c^+_{3_\uparrow} c^+_{4_\downarrow} c^+_{5_\downarrow} c^+_{6_\downarrow}\rangle\,, & \hat{\mathrm{P}}|A'_5\rangle = |A'_1\rangle &= |\mathrm{c}^+_{2_\uparrow} c^+_{3_\downarrow} c^+_{4_\uparrow} c^+_{5_\downarrow} c^+_{6_\downarrow}\rangle\,.
\end{aligned}$$

This shows us that we have five configurations in total that can be created

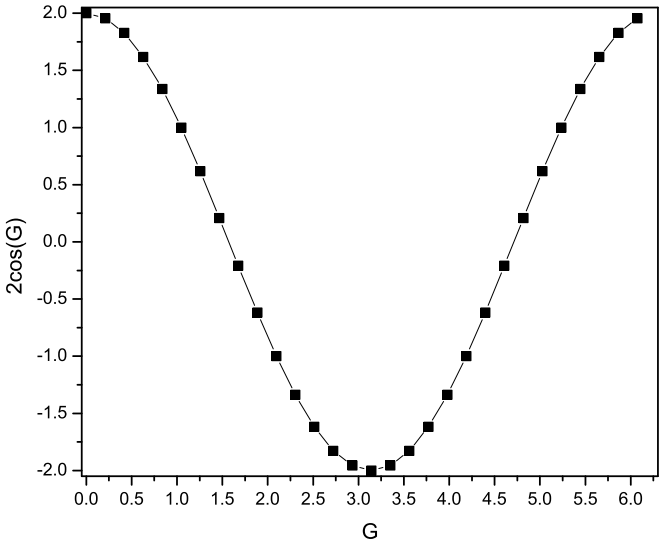

a)

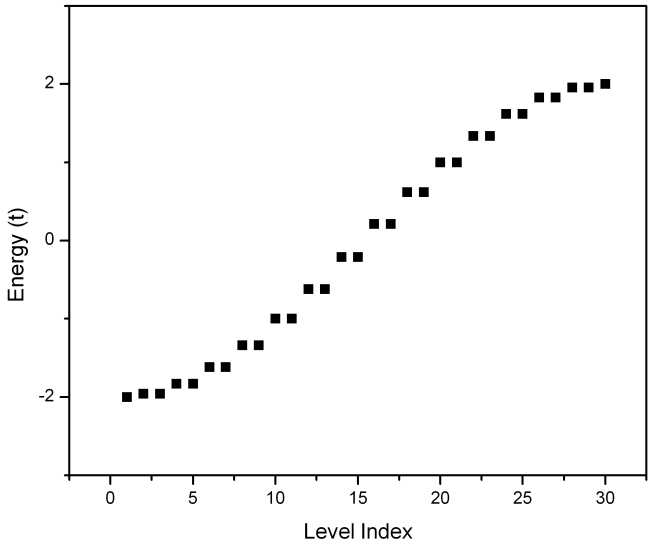

b)

Figure 7: a) Allowed energy levels as a function of the wavevector $G = Q + \kappa/6$. b) Allowed energy levels graphed against eigenvalue index to show where degeneracies occur. These degeneracies come from the circular symmetry of the ring.

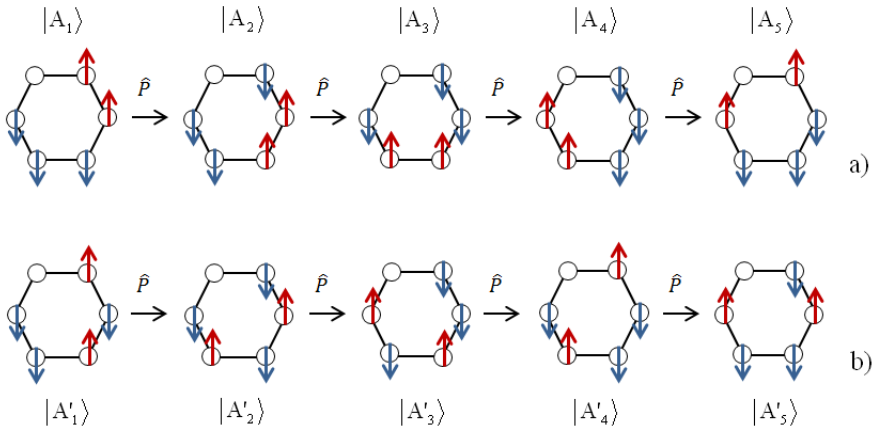

Figure 8: The permutation operator acting on a five electron system with no double occupation in the a) first subspace and the b) second subspace.

by the permutation operator for each subspace for each hole position. These two are non interacting due to the inability to reproduce a configuration from one subspace into another using the operator $\hat{\mathrm{P}}$, while these two subspaces together reproduce the whole Hilbert space. To create our new basis, we create a linear combination of these states, within each subspace, that we then use to create our Hamiltonian matrix:

$$|\Phi_{j_1 j_2 ... j_n}(\kappa; \sigma_1 \sigma_2 ... \sigma_n)\rangle = \left[\frac{1}{\sqrt{n'}} \sum_{m=0}^{n'-1} e^{Imk} c^{+}_{j_1 p^m(\sigma_1)} ... c^{+}_{j_n p^m(\sigma_n)} \right] |0\rangle \ , \tag{38}$$

where n' is the number of configurations possible using the permutation operator $\hat{\mathrm{P}}$, j_n is the position of the created electron, and $p^m(\sigma_n)$ is the permutation operator acting m times on a spin σ_n. Adding in the condition for orthogonality we see that $\kappa = \frac{2\pi}{5} n$, $n = 0, 1, ..., 4$. Using these new states in combination with Eq.1 we

can create our full Hamiltonian as:

$$H = \begin{bmatrix}
0 & +t & 0 & 0 & 0 & +te^{-I\kappa} & 0 & 0 & 0 & 0 & 0 & 0 \\
+t & 0 & +t & 0 & 0 & 0 & 0 & 0 & 0 & 0 & 0 & 0 \\
0 & +t & 0 & +t & 0 & 0 & 0 & 0 & 0 & 0 & 0 & 0 \\
0 & 0 & +t & 0 & +t & 0 & 0 & 0 & 0 & 0 & 0 & 0 \\
0 & 0 & 0 & +t & 0 & +t & 0 & 0 & 0 & 0 & 0 & 0 \\
+te^{+I\kappa} & 0 & 0 & 0 & +t & 0 & 0 & 0 & 0 & 0 & 0 & 0 \\
0 & 0 & 0 & 0 & 0 & 0 & 0 & +t & 0 & 0 & 0 & +te^{-I\kappa} \\
0 & 0 & 0 & 0 & 0 & 0 & +t & 0 & +t & 0 & 0 & 0 \\
0 & 0 & 0 & 0 & 0 & 0 & 0 & +t & 0 & +t & 0 & 0 \\
0 & 0 & 0 & 0 & 0 & 0 & 0 & 0 & +t & 0 & +t & 0 \\
0 & 0 & 0 & 0 & 0 & 0 & 0 & 0 & 0 & +t & 0 & +t \\
0 & 0 & 0 & 0 & 0 & 0 & +te^{+I\kappa} & 0 & 0 & 0 & +t & 0
\end{bmatrix}.$$

Here we see that the two subspaces are independent of each other and that they are degenerate. These blocks we can see are the exact solution to the $S_z = \frac{3}{2}$ case, therefore we have the same eigenvalues and eigenstates.

Unfortunately using this method we cannot identify the total spin states using the permutation operator $\hat{\mathrm{P}}$ as we can with the S^2 operator, $\hat{S^2} = \frac{N}{2} + S_z^2 - \sum_{ij} c_{j\uparrow}^+ c_{i\downarrow}^+ c_{j\downarrow} c_{i\uparrow}$, where N is the number of electrons in the ABR, and S_z is the representation of the number of spin-up and spin-down electrons in the system. This is required as the spin projections $S_z = \frac{3}{2}$ and $S_z = \frac{1}{2}$ contain total spin configurations of $S = \frac{5}{2}$, $\frac{3}{2}$, and $S = \frac{5}{2}$, $\frac{3}{2}$, $\frac{1}{2}$ respectively. Therefore, to separate the total spin configurations from the spin projections we turn to "spin currents". To do this we first define a spin current operator[45]:

$$\hat{J}_n = \sum_j e^{I\kappa_n j} c^+_{j\uparrow} c_{j\downarrow} \, , \kappa_n = \frac{2\pi}{5} n \, , n = \{1,2,3,4,5\} \ . \tag{39}$$

This operator will take an electron, flip its spin, and shuffle it through the occupied sites to obtain an expression for a state of a minority spin electron in the ring.

Therefore: $\hat{J}_n \left| c^+_{2\downarrow} c^+_{3\downarrow} c^+_{4\downarrow} c^+_{5\downarrow} c^+_{6\downarrow} \right\rangle = e^{I\kappa_n} \left| c^+_{2\uparrow} c^+_{3\downarrow} c^+_{4\downarrow} c^+_{5\downarrow} c^+_{6\downarrow} \right\rangle + e^{I2\kappa_n} \left| c^+_{3\uparrow} c^+_{2\downarrow} c^+_{4\downarrow} c^+_{5\downarrow} c^+_{6\downarrow} \right\rangle +$

$e^{I3\kappa_n} \left| c^+_{4\uparrow} c^+_{2\downarrow} c^+_{3\downarrow} c^+_{5\downarrow} c^+_{6\downarrow} \right\rangle + e^{I4\kappa_n} \left| c^+_{5\uparrow} c^+_{2\downarrow} c^+_{3\downarrow} c^+_{4\downarrow} c^+_{6\downarrow} \right\rangle + e^{I5\kappa_n} \left| c^+_{6\uparrow} c^+_{2\downarrow} c^+_{3\downarrow} c^+_{4\downarrow} c^+_{5\downarrow} \right\rangle$.

This is an example of using this spin current operator once, but as we have two spins flipped we need to apply this operator twice: $\hat{J}_n \hat{J}_m \left| c^+_{2\downarrow} c^+_{3\downarrow} c^+_{4\downarrow} c^+_{5\downarrow} c^+_{6\downarrow} \right\rangle$.

With this expression it would seem as though we would have 25 terms, five possible configurations for each of the two independent indices, each with $25(\kappa_1 \cdot \kappa_2)$ states. However, we only have 10 unique configurations of i,j indices, this comes from five of the 25 states being nonexistent: $c^+_{i\uparrow} c_{i\downarrow} c^+_{j\uparrow} c_{j\downarrow} = 0$ when $i = j$, and the remaining 20 being just 10 due to $c^+_{i\uparrow} c_{i\downarrow} c^+_{j\uparrow} c_{j\downarrow} = c^+_{j\uparrow} c_{j\downarrow} c^+_{i\uparrow} c_{i\downarrow}$. Next, looking at the spin current states we see that $\kappa_1 + \kappa_2 = \kappa_2 + \kappa_1$ which means that ordering is irrelevant, which leaves us with 15 states remaining. This leaves us with the same subspaces as we had in figure 8 and the permutation operator method, which we define as A and A'.

$$\hat{J}_n \hat{J}_m \left| c^+_{2\downarrow} c^+_{3\downarrow} c^+_{4\downarrow} c^+_{5\downarrow} c^+_{6\downarrow} \right\rangle = \sum_n \sum_m \left(e^{I(\kappa_n n + \kappa_m m)} c^+_{n\uparrow} c_{n\downarrow} c^+_{m\uparrow} c_{m\downarrow} \right) \left| c^+_{2\downarrow} c^+_{3\downarrow} c^+_{4\downarrow} c^+_{5\downarrow} c^+_{6\downarrow} \right\rangle \ . \tag{40}$$

Here $|A_n\rangle$ and $|A'_n\rangle$ are the unique configuration subspaces:

$$|\mathrm{A}_1\rangle = |\mathrm{c}^+_{2\uparrow}c^+_{3\uparrow}\rangle|c^+_{4\downarrow}c^+_{5\downarrow}c^+_{6\downarrow}\rangle\,, \quad |A'_1\rangle = |\mathrm{c}^+_{2\uparrow}c^+_{4\uparrow}\rangle|c^+_{3\downarrow}c^+_{5\downarrow}c^+_{6\downarrow}\rangle\,,$$

$$|\mathrm{A}_2\rangle = |\mathrm{c}^+_{3\uparrow}c^+_{4\uparrow}\rangle|c^+_{2\downarrow}c^+_{5\downarrow}c^+_{6\downarrow}\rangle\,, \quad |A'_2\rangle = |\mathrm{c}^+_{3\uparrow}c^+_{5\uparrow}\rangle|c^+_{2\downarrow}c^+_{4\downarrow}c^+_{6\downarrow}\rangle\,,$$

$$|\mathrm{A}_3\rangle = |\mathrm{c}^+_{4\uparrow}c^+_{5\uparrow}\rangle|c^+_{2\downarrow}c^+_{3\downarrow}c^+_{6\downarrow}\rangle\,, \quad |A'_3\rangle = |\mathrm{c}^+_{4\uparrow}c^+_{6\uparrow}\rangle|c^+_{2\downarrow}c^+_{3\downarrow}c^+_{5\downarrow}\rangle\,,$$

$$|\mathrm{A}_4\rangle = |\mathrm{c}^+_{5\uparrow}c^+_{6\uparrow}\rangle|c^+_{2\downarrow}c^+_{3\downarrow}c^+_{4\downarrow}\rangle\,, \quad |A'_4\rangle = |\mathrm{c}^+_{2\uparrow}c^+_{5\uparrow}\rangle|c^+_{3\downarrow}c^+_{4\downarrow}c^+_{6\downarrow}\rangle\,,$$

$$|\mathrm{A}_5\rangle = |\mathrm{c}^+_{2\uparrow}c^+_{6\uparrow}\rangle|c^+_{3\downarrow}c^+_{4\downarrow}c^+_{5\downarrow}\rangle\,, \quad |A'_5\rangle = |\mathrm{c}^+_{3\uparrow}c^+_{6\uparrow}\rangle|c^+_{2\downarrow}c^+_{4\downarrow}c^+_{5\downarrow}\rangle\,.$$

To separate the configurations by total spin, we first divide the configurations according to their total spin current, $\kappa_1 + \kappa_2$, this gives us five subspaces.

$\kappa_1+\kappa_2=1$	$\kappa_1+\kappa_2=2$	$\kappa_1+\kappa_2=3$	$\kappa_1+\kappa_2=4$	$\kappa_1+\kappa_2=5$
{1,5}	{2,5}	{3,5}	{4,5}	{5,5}
{3,3}	{1,1}	{4,4}	{2,2}	{1,4}
{2,4}	{3,4}	{1,2}	{1,3}	{2,3}

Figure 9: Table of our total spin currents within individual subspaces, where the numbers in brackets are κ_1 or κ_2.

Applying the $\hat{S}^2$ operator to these states, we find that all $\kappa_2 = 5$ states, where $\kappa_1 \neq 5$, are $S = \frac{3}{2}$ and the state with both $\kappa_1 = 5$ and $\kappa_2 = 5$ is $S = \frac{5}{2}$. However when the $\hat{S}^2$ operator is applied to all the remaining states we find that they are not eigenfunctions of the $\hat{S}^2$ operator, and are also not orthogonal within their subspace. To solve this, we use the Gram-Schmidt method to orthogonalize the states with no definite spin[45]. This is done by taking the state and subtracting off its projection onto the higher spin state.

$$|\frac{1}{2}{}^{h}_{\kappa_{tot}}\rangle = |1^h_{\kappa_{tot}}\rangle - \langle 1^h_{\kappa_{tot}}|\frac{x}{2}{}^{h}_{\kappa_{tot}}\rangle|\frac{x}{2}{}^{h}_{\kappa_{tot}}\rangle\,, \tag{41}$$

where $|\frac{1}{2}{}^{h}_{\kappa_{tot}}\rangle$ is the newly obtained orthogonal $S = \frac{1}{2}$ state in the h, κ_{tot} subspace, where h is the position of the hole. $|1^h_{\kappa_{tot}}\rangle$ is the non orthogonal state that we are

looking to create a $|\frac{1}{2}{}^{h}_{\kappa_{tot}}\rangle$ out of, and $|\frac{x}{2}{}^{h}_{\kappa_{tot}}\rangle$ is the $\frac{3}{2}$ or $\frac{5}{2}$ state within the subspace that we are removing from the projection of the $|1^{h}_{\kappa_{tot}}\rangle$ state. We find that the states that had no definite spin are the same state, within their subspace, this leaves us with only five $S = \frac{1}{2}$ states. We can then make our total S states out of a linear combination of $|A\rangle$ and $|A'\rangle$ states we created earlier, as well as expanding and simplifying equation (40).

$$|J^{h}_{\kappa_{tot}}\rangle = \frac{1}{N}\sum_{n} e^{I\kappa_{tot}n}([e^{I\kappa_1} + e^{I\kappa_2}]\,|A_n\rangle + [e^{I2\kappa_1} + e^{I2\kappa_2}]\,|A'_n\rangle)\,, \tag{42}$$

where the normalization factor N is equal to $2\sqrt{10}$ for $\kappa_1 = \kappa_2$ and $\sqrt{15}$ for $\kappa_1 \neq \kappa_2$. This form is the consequence of using the spin current operator twice on the subspaces A and A'. The phases κ_1 and κ_2 track the two minority carriers in the configurations, which is why for the B subspace we have a factor of 2 in the phase, as the two carriers are separated by a majority carrier whereas the common phase factor is due to there being two minority carriers in both subspaces. Performing this rotation for every position of the hole gives us a block diagonal Hamiltonian, ten 6x6 blocks for a hole moving in a certain total spin and total current subspace. This Hamiltonian matrix is the same as we have found in the previous subsection although now we have separated the subspaces by total spin.

3.3.2 Results of Direct Diagonalization for Finite U and V

Now that we have the simplified case solved, we reintroduce electron-electron interactions into the system and re-allow double occupation. To take into account the interactions in our system, we look at the Fourier transformed Hamiltonian in equation (17) and solve for all configurations for a given S_z. We look specifically

at how the ground states of the different total spin configurations are affected by changes in Coulomb interaction. figures 10 and 11 show how the total spin ground states evolve as U/t and V/t change, and how at high U/t (in this case $U/t = 70$), there is a crossing of the $S = \frac{3}{2}$ ground state with the $S = \frac{5}{2}$ ground state resulting in a reordering of the excited states of the system. Whereas for changes in V/t we notice no such change in the system, but rather that the splitting between the states seems to widen.

As we can see in figure 10a, the ground state energy of the five electron system is ordered as $S = \frac{1}{2}$, $S = \frac{3}{2}$, and $S = \frac{5}{2}$ for $U \neq 0$. But as the interaction energy U is increased we see the $S = \frac{1}{2}$ ground state approach the $S = \frac{5}{2}$ state, while the $S = \frac{3}{2}$ is now the highest energy state.

3.4 Quarter Filled Case (Three Electrons)

3.4.1 Orthogonal Basis ($\hat{S}^2$)

To create the quarter filled case we chose to create an orthogonal basis that would allow us to separate the total spin. We do this by using the total spin operator, $\hat{S}^2$. The three electron case has two unique S_z configurations, either the spin polarized case, which is clearly an eigenstate of $\hat{S}^2$, and the spin depolarized case which contains both total $S = \frac{3}{2}$ and $S = \frac{1}{2}$ configurations and therefore has to have the higher spin state separated out. By applying the $\hat{S}^2$ operator on the $S_z = \frac{1}{2}$ case, and then diagonalizing the corresponding matrix, we get the orthogonal basis,

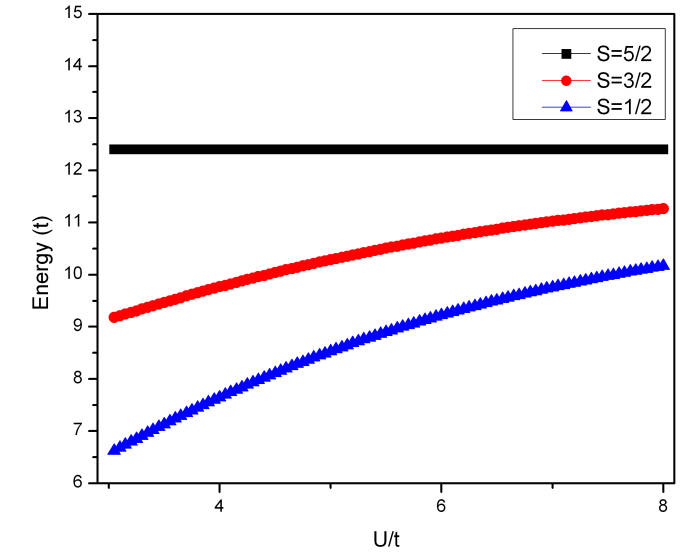

a)

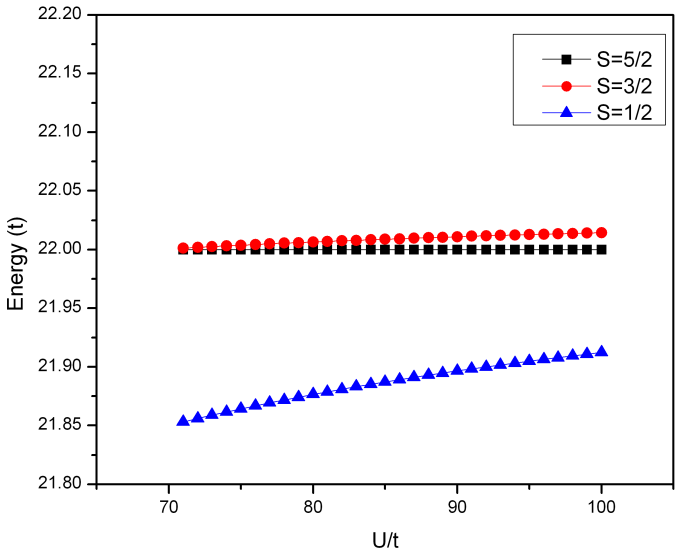

b)

Figure 10: Five electron case with V = 3: a) Ground state versus change of U/t. b) Close up of the ground state versus U/t to show a crossing of the $S = \frac{3}{2}$ state with $S = \frac{5}{2}$.

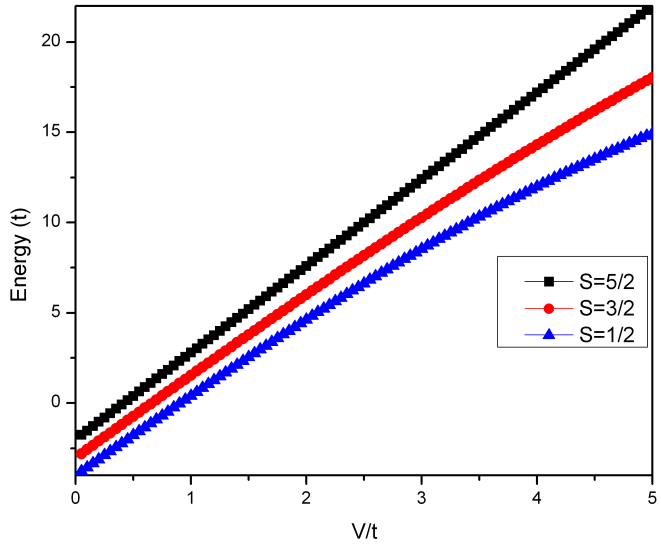

Figure 11: Five electron case with U = 5: Ground state versus change of V/t.

$$
\begin{aligned}
|A\rangle &= \frac{1}{\sqrt{3}}\left(\left|c^{+}_{1^{st}\uparrow}c^{+}_{2^{nd}\uparrow}c^{+}_{3^{rd}\downarrow}\right\rangle + \left|c^{+}_{1^{st}\uparrow}c^{+}_{2^{nd}\downarrow}c^{+}_{3^{rd}\uparrow}\right\rangle + \left|c^{+}_{1^{st}\downarrow}c^{+}_{2^{nd}\uparrow}c^{+}_{3^{rd}\uparrow}\right\rangle\right), \\
|B\rangle &= \frac{1}{\sqrt{6}}\left(\left|c^{+}_{1^{st}\uparrow}c^{+}_{2^{nd}\uparrow}c^{+}_{3^{rd}\downarrow}\right\rangle - 2\left|c^{+}_{1^{st}\uparrow}c^{+}_{2^{nd}\downarrow}c^{+}_{3^{rd}\uparrow}\right\rangle + \left|c^{+}_{1^{st}\downarrow}c^{+}_{2^{nd}\uparrow}c^{+}_{3^{rd}\uparrow}\right\rangle\right), \\
|C\rangle &= \frac{1}{\sqrt{2}}\left(\left|c^{+}_{1^{st}\uparrow}c^{+}_{2^{nd}\uparrow}c^{+}_{3^{rd}\downarrow}\right\rangle - \left|c^{+}_{1^{st}\downarrow}c^{+}_{2^{nd}\uparrow}c^{+}_{3^{rd}\uparrow}\right\rangle\right).
\end{aligned}
$$

$|A\rangle$ is the higher spin state with $S = \frac{3}{2}$ and the other two are in the two orthogonal subspaces with $S = \frac{1}{2}$. This notation is used for the singly occupied configurations, with the convention that the lowest numbered dot goes to the left most position and gets higher the farther right you go. For the doubly occupied configurations we only have one spin configuration since the up and down spin electrons on the same dot are indistinguishable. Therefore we have just a convention we follow which has the doubly occupied configurations defined by their double occupancy,

eg. $\left|c^+_{3_\downarrow} c^+_{3_\uparrow} c^+_{2_\uparrow}\right\rangle$. We then solve for the eigenenergies by running through the interactions between all possible configurations, and subspaces, to fill our Hamiltonian matrix.

3.4.2 Results of Direct Diagonalization for Finite U and V

Looking at the ground state energies of the two configurations as a function of U/t and V/t we see that for small interaction energy, the $S = \frac{1}{2}$ state is the ground state of the system. As we increase U, we notice that there is a crossing between the $S = \frac{1}{2}$ and the $S = \frac{3}{2}$ states leading to $S = \frac{3}{2}$ being the new ground state, as shown in figure 12. When looking outside of realistic conditions ($V > U$), we can see a double crossing of the ground state (figure 13.), where due to a high value of U the ground state of the system changes from $S = \frac{1}{2}$ to $S = \frac{3}{2}$, however as V/t increases $S = \frac{1}{2}$ again becomes the ground state. This is due to a change of the ground state of $S = \frac{1}{2}$ from its initial ground state to one of its excited states due to the increase of interaction energy. This change of ground state is accompanied with a shift in the total angular momentum of the system from $\frac{\pi}{3}$ to 0 (figure 13.).

4 Optical Properties of the Artificial Benzene Ring

4.1 Dipole Approximation and Fermi's Golden Rule

For absorption of light by the ABR we use Fermi's golden rule. This is used for calculating the transition rate from the lowest energy eigenstate to excited, higher energy eigenstates due to the absorption of a photon, which we take as a

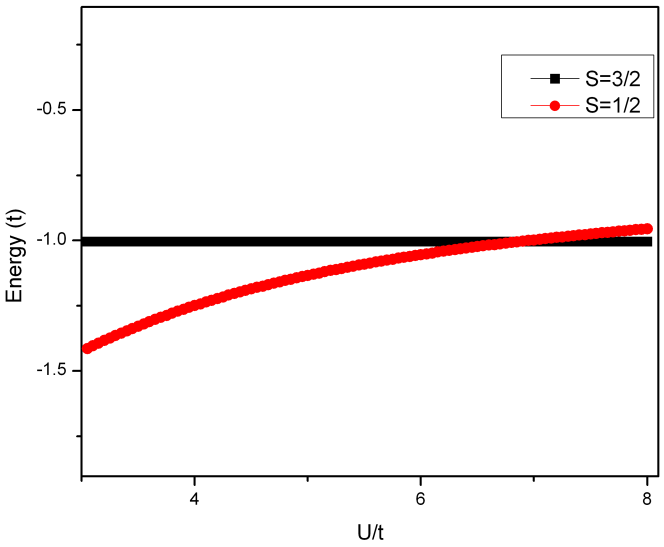

a)

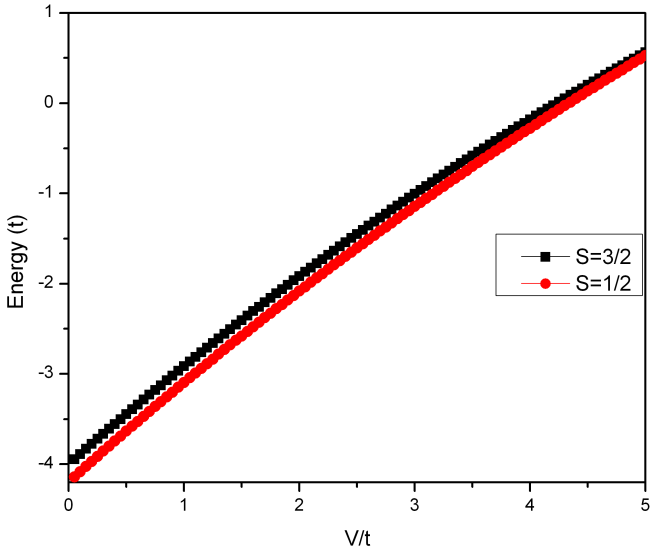

b)

Figure 12: Three electron case: a) Ground state versus change of U/t, with V = 3. b) Ground state versus change of V/t, with U = 5.

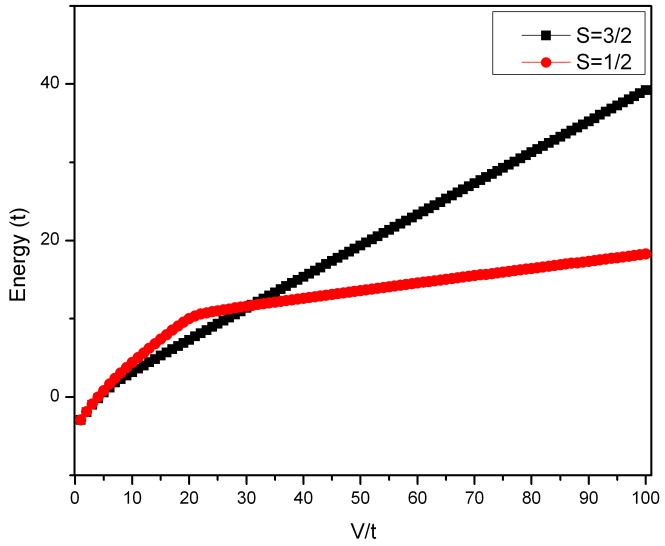

a)

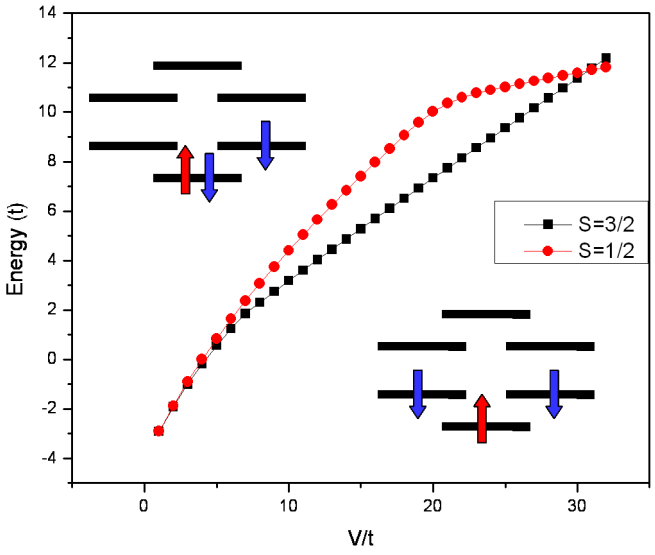

b)

Figure 13: Three electron case with U = 5: a) Ground state versus change of V/t with V being greater than U (hence unrealistic situation). b) Ground state versus change of V/t close up where we can see a double crossing of the ground states.

perturbation.

$$I_{GSf}(w) = \sum_f \left| \langle f | \hat{P}^+ | GS \rangle \right|^2 \delta \left(E_f - E_{GS} - w \right) \ . \tag{43}$$

Here I_{GSF} is the intensity of the transition from the groundstate to a final excited state. P is the polarization operator given by:

$$\hat{P}^+ = \sum_{pq\sigma} d\left(p,q\right) b^+_{p\sigma} b_{q\sigma} \ , \tag{44}$$

where p and q are Fourier basis states. The dipole moment $d(p,q)$ is defined by[46]:

$$d(p,q) = \langle p | \, \vec{\varepsilon} \cdot \vec{r} \, | q \rangle = \sum_{i=1}^{N} \sum_{j=1}^{N} A^*_{p,i} A_{q,j} \, \langle i | \, \vec{\varepsilon} \cdot \vec{r} \, | j \rangle \ , \tag{45}$$

where the coefficients $A^*_{p,i}$ and $A_{q,j}$ are the Fourier transform coefficients. We next solve for the dipole element, $\langle i | \, \vec{\varepsilon} \cdot \vec{r} \, | j \rangle$, by evaluating it in the basis of localized orbitals $\psi(\vec{r} - \vec{R}_i)$. We have:

$$\langle i | \, \vec{\varepsilon} \cdot \vec{r} \, | j \rangle = \vec{\varepsilon} \cdot \int d\vec{r} \psi^* \left(\vec{r} - \vec{R}_i \right) \vec{r} \psi \left(\vec{r} - \vec{R}_j \right) \ . \tag{46}$$

Replacing $\vec{r} \rightarrow \vec{r} + \vec{R}_i$,

$$\begin{aligned} \langle i | \vec{\varepsilon} \cdot \vec{r} | j \rangle &= \vec{\varepsilon} \cdot \int d\vec{r} \psi^*(\vec{r}) (\vec{r} + \vec{R}_i) \psi \left(\vec{r} - (\vec{R}_j - \vec{R}_i) \right) \ , & (47) \\ \langle i | \vec{\varepsilon} \cdot \vec{r} | j \rangle &= \vec{\varepsilon} \cdot \int d\vec{r} \psi^* \left(\vec{r} \right) \vec{r} \psi \left(\vec{r} - (\vec{R}_j - \vec{R}_i) \right) \\ &+ \vec{\varepsilon} \cdot \vec{R}_i \int d\vec{r} \psi^*(\vec{r}) \psi \left(\vec{r} - (\vec{R}_j - \vec{R}_i) \right) \ . & (48) \end{aligned}$$

Using the orthogonality of the orbitals, and using our constraint for nearest neighbor interactions only, we get our dipole interactions between p_z orbitals as[47]:

$$\langle i | \, \vec{\varepsilon} \cdot \vec{r} \, | j \rangle = D \vec{\varepsilon} \cdot (\hat{R}_j - \hat{R}_i) \delta_{\langle ij \rangle} + \vec{\varepsilon} \cdot \hat{R}_i \delta_{ij} \ , \tag{49}$$

where $D = \left| \int d\vec{r} \phi_z^* (\vec{r}) \, \vec{r} \phi_z \left(\vec{r} - \vec{R}_{\langle ij \rangle} \right) \right| = 0.3433$ in units of nearest neighbor distance, where ϕ_z is the three dimensional Slater p_z orbital that we exchanged for our state ψ[46].

Following Ozfidan[45], we rotate out of on-site notation into the molecular orbital notation through Fourier transformation:

$$|q\rangle = \frac{1}{\sqrt{6}} \sum_{j=0}^{5} e^{Iqj} |j\rangle \ . \tag{50}$$

We will consider circularly polarized light, therefore we use $\varepsilon_\pm$ where: $\vec{\varepsilon}_\pm \cdot \vec{R}_m = |R| \, e^{\pm I \frac{2\pi}{6} m}$ and so:

$$\begin{aligned} \langle p | \, \vec{\varepsilon}_\pm \cdot \vec{r} \, | q \rangle &= \frac{1}{\sqrt{6}} \sum_{i=0}^{5} e^{-Ipi} \frac{1}{\sqrt{6}} \sum_{j=0}^{5} e^{Iqj} \langle i | \, \vec{\varepsilon}_\pm \cdot \vec{r} \, | j \rangle \ , & (51) \\ \langle p | \, \vec{\varepsilon}_\pm \cdot \vec{r} \, | q \rangle &= \frac{1}{6} \sum_{i=0}^{5} \sum_{j=0}^{5} e^{I(qj - pi)} \left[D \, |R| \left(e^{\pm I \frac{2\pi}{6} j} - e^{\pm I \frac{2\pi}{6} i} \right) \delta_{\langle ij \rangle} \right. \\ &+ \left. |R| \, e^{\pm I \frac{2\pi}{6} i} \delta_{ij} \right] \ . & (52) \end{aligned}$$

We next limit the summation to only nearest neighbors, which forces $i = j \pm 1$, and we simplify:

$$\langle p | \, \vec{\varepsilon}_\pm \cdot \vec{r} \, | q \rangle = \frac{|R|}{6} \sum_{j=0}^{5} e^{Ij\left(q - p \pm \frac{\pi}{3}\right)} \left[1 + 2D \left(cos \left(\left(p \pm \frac{\pi}{3} \right) \right) - cos \left(p \right) \right) \right] \ . \tag{53}$$

This summation is only nonzero for $p = q \pm \frac{\pi}{3}$,

$$\langle p | \, \vec{\varepsilon}_\pm \cdot \vec{r} \, | q \rangle = |R| \left[1 + 2D \left(cos \left(\left(p \pm \frac{\pi}{3} \right) \right) - cos \left(p \right) \right) \right] \delta \left(q - p \pm \frac{\pi}{3} \right) \ , \tag{54}$$

$$\langle p | \, \vec{\varepsilon}_\pm \cdot \vec{r} \, | q \rangle = C \cdot \delta \left(q - p \pm \frac{\pi}{3} \right) \ . \tag{55}$$

C is a constant in front of the selection rules δ. Therefore we now have selection rules in the dipole allowed transitions during the absorption of a photon.

4.2 Simplified Model of Absorption Spectrum Without Interactions

4.2.1 Lowest Energy Excitations for Half Filled ABR

To start we look at a simplified case to be able to develop some intuition. We do this by looking at the eight lowest excitations available from the ground state of our half filled case with interactions turned off (figure 14.). The first two configurations of each row of excited states are dark states because the electron is moved within the same rotational subspace with a change in total angular momentum of π, whereas the dipole allowed excitations have a change in angular momentum of $\frac{\pi}{3}$. This gives us a total of four bright states and four dark ones when the electron-electron interactions are turned off.

4.2.2 Singlet and Triplet Excitons

To solve for the optical spectra we generate configurations by exciting spin-down and spin-up electrons, $|A_n\rangle$ and $|B_n\rangle$, respectively shown in figure 14.

	1st class		2nd class
$\|\mathrm{A}_1\rangle =$	$\|\mathrm{b}^+_{1_\uparrow} b^+_{2_\uparrow} b^+_{3_\uparrow}\rangle \|b^+_{1_\downarrow} b^+_{2_\downarrow} b^+_{5_\downarrow}\rangle$,	$\|\mathrm{B}_1\rangle =$	$\|\mathrm{b}^+_{1_\uparrow} b^+_{2_\uparrow} b^+_{5_\uparrow}\rangle \|b^+_{1_\downarrow} b^+_{2_\downarrow} b^+_{3_\downarrow}\rangle$,
$\|\mathrm{A}_2\rangle =$	$\|\mathrm{b}^+_{1_\uparrow} b^+_{2_\uparrow} b^+_{3_\uparrow}\rangle \|b^+_{1_\downarrow} b^+_{2_\downarrow} b^+_{4_\downarrow}\rangle$,	$\|\mathrm{B}_2\rangle =$	$\|\mathrm{b}^+_{1_\uparrow} b^+_{2_\uparrow} b^+_{4_\uparrow}\rangle \|b^+_{1_\downarrow} b^+_{2_\downarrow} b^+_{3_\downarrow}\rangle$,
$\|\mathrm{A}_3\rangle =$	$\|\mathrm{b}^+_{1_\uparrow} b^+_{2_\uparrow} b^+_{3_\uparrow}\rangle \|b^+_{1_\downarrow} b^+_{3_\downarrow} b^+_{4_\downarrow}\rangle$,	$\|\mathrm{B}_3\rangle =$	$\|\mathrm{b}^+_{1_\uparrow} b^+_{3_\uparrow} b^+_{4_\uparrow}\rangle \|b^+_{1_\downarrow} b^+_{2_\downarrow} b^+_{3_\downarrow}\rangle$,
$\|\mathrm{A}_4\rangle =$	$\|\mathrm{b}^+_{1_\uparrow} b^+_{2_\uparrow} b^+_{3_\uparrow}\rangle \|b^+_{1_\downarrow} b^+_{3_\downarrow} b^+_{5_\downarrow}\rangle$,	$\|\mathrm{B}_4\rangle =$	$\|\mathrm{b}^+_{1_\uparrow} b^+_{3_\uparrow} b^+_{5_\uparrow}\rangle \|b^+_{1_\downarrow} b^+_{2_\downarrow} b^+_{3_\downarrow}\rangle$.

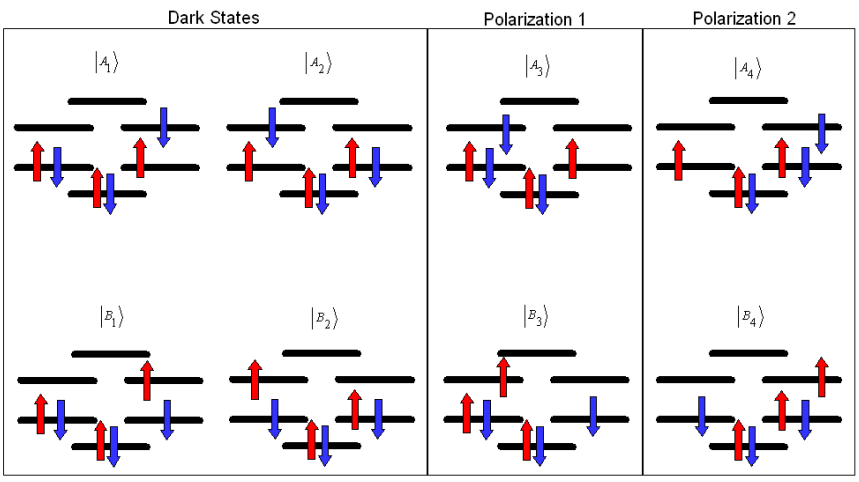

Figure 14: The lowest energy excitations from the ground state of neutral ABR. Polarization 1 and 2 are left circularly polarized light and right circularly polarized light respectively.

To find the absorption intensity we compare each of these above configurations with each other, requiring the movement of one electron to be identical. Those with one electron differences between configurations contribute non zero elements to the 8x8 dipole matrix by using equation (54), which compares the different electron states to see if the movement of the electron is valid in creating a dipole, and gives a relative intensity between those configurations. Let us consider an electron being excited from the ground state, i.e., $|GS\rangle = |1_\uparrow 2_\uparrow 3_\uparrow 1_\downarrow 2_\downarrow 3_\downarrow\rangle$, to the excited state $|A_1\rangle$. Here the electron moves from an energy level with angular momentum $\frac{\pi}{3}$ to one with $\frac{-2\pi}{3}$. According to our selection rules in equation (54), this will result in a dipole element of zero. Next let us consider an excitation to $|A_3\rangle$, where the electron moves from an energy level with angular momentum $\frac{\pi}{3}$ to one with $\frac{2\pi}{3}$. This is an allowed transition according to the selection rules, therefore we evaluate the dipole matrix element.

$$\left\langle \frac{2\pi}{3} \middle| \vec{\varepsilon}_{\pm} \cdot \vec{r} \middle| \frac{\pi}{3} \right\rangle = |R| \left[1 + 2D \left(cos\left((\pi) \right) \right. \right.$$
$$\left. \left. - \; cos(\frac{2\pi}{3}) \right) \right] \delta \left(\frac{\pi}{3} - \frac{2\pi}{3} + \frac{\pi}{3} \right) , \tag{56}$$

$$\left\langle \frac{2\pi}{3} \middle| \vec{\varepsilon}_{\pm} \cdot \vec{r} \middle| \frac{\pi}{3} \right\rangle = 1 + 2D(-1 + 0.5) , \tag{57}$$

$$\left\langle \frac{2\pi}{3} \middle| \vec{\varepsilon}_{\pm} \cdot \vec{r} \middle| \frac{\pi}{3} \right\rangle = 0.656476 . \tag{58}$$

This method is used to fill our dipole matrix; we can then use equation (43) to find all of the intensities of transitions from the ground state to the excited states. Turning Coulomb interactions on, we have a mixing of configurations. This mixing creates singlets and triplets out of the different configurations, i.e., $\frac{1}{\sqrt{2}}\Big(|A_1\rangle \pm |B_1\rangle \Big)$. Only singlets are optically active. Now that we have a good idea of how the simple case works we can expand to the full system.

4.3 Charge Neutral Optical Case

For the half filled case we looked at the $S = \frac{1}{2}$ state, this is due to this spin state being the ground state for the six electron case. For small interactions it can be seen (figure 15 left.), that the simplified model, section 4.2, is a good approximation as we only expected a single peak in each polarization and this is indeed what we observe at low U. As the interaction energy U is increased we observe the creation of Hubbard bands (figure 15 right.), which represent the amount of doubly occupied dots in the system. These bands have a separation from each other that is based on the interaction energy U, since it costs more energy to doubly occupy a dot.

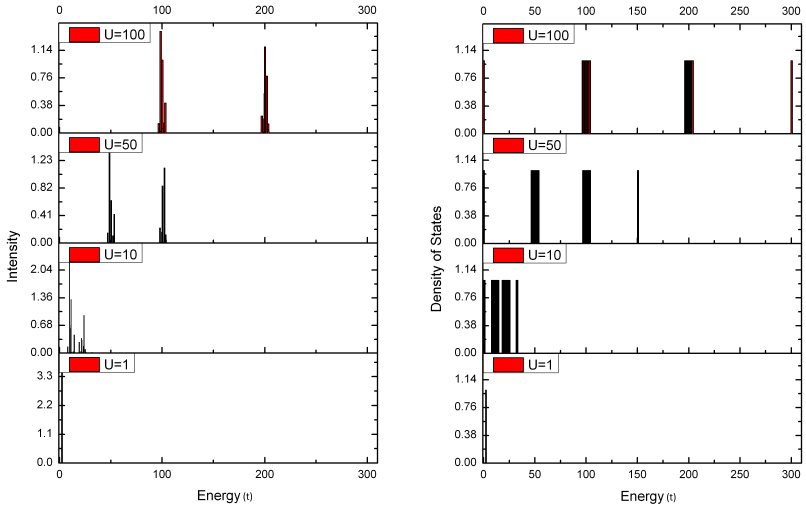

Figure 15: Absorption spectrum of charge neutral ABR, with V = 0: Absorption spectrum for values of U ranging from 1 to 100, we have the intensities and the energy levels side by side to show which are bright.

4.4 Charged Optical Case

4.4.1 S=5/2 Case

We then look at the charged ABR case. For the spin 5/2 case we have the same result as for the simplified case, i.e., we have one intensity peak in each polarization.

4.4.2 S=3/2 Case

For the 3/2 case we have, as in the six electron case, a splitting into Hubbard bands.

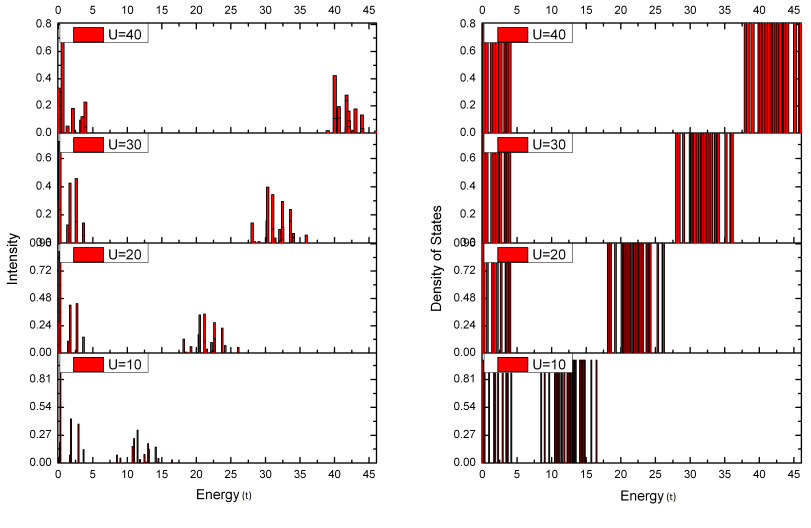

a)

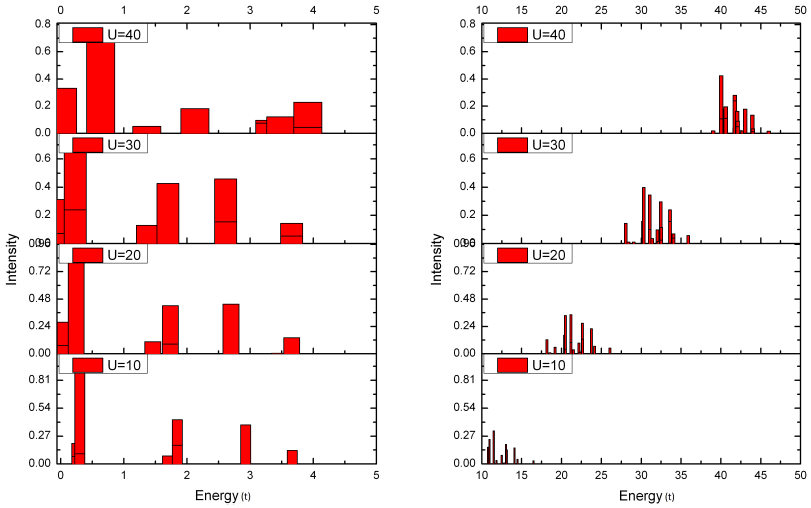

b)

Figure 16: Absorption spectrum of charged ABR, $S = 3/2$, with V = 0: a) Absorption spectrum for values of U ranging from 10 to 40, we have the intensities and the energy levels side by side to show which are bright. b) Magnified look at two of the lowest Hubbard bands.

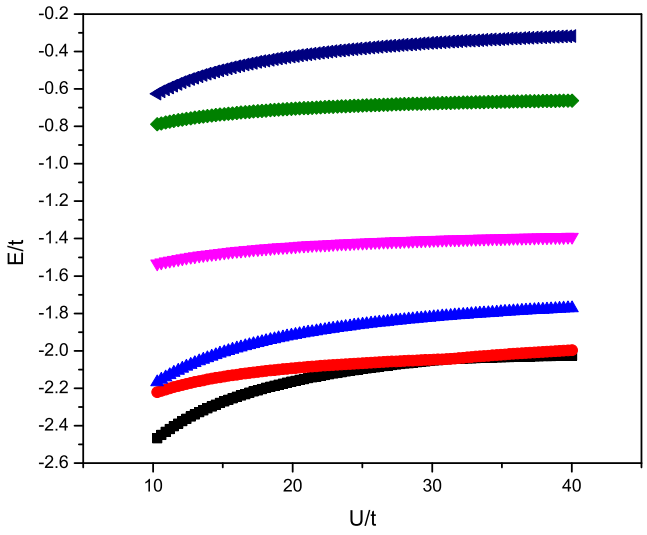

a)

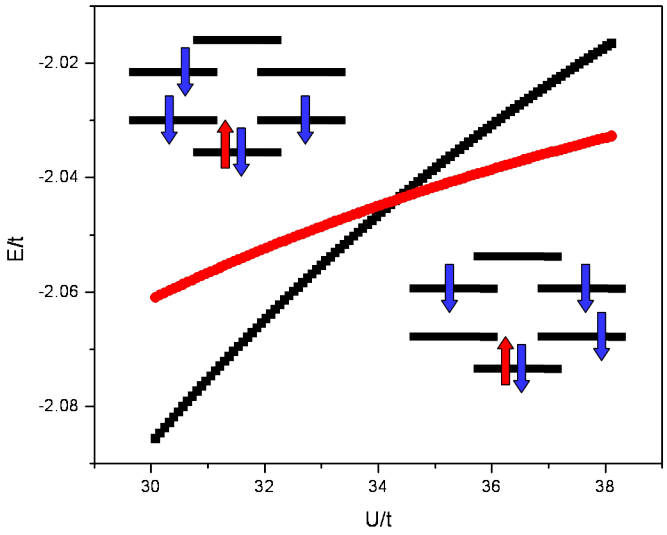

b)

Figure 17: Five electron spin 3/2 case, with V = 0: a) Ground state and first five excited energy levels changing with respect to U/t. b) Magnified portion of U/t = 30 to 38 to show the crossing of an excited state with the ground state, the dominant configurations for the states are shown, with the original ground state on the left, and the new one on the right.

4.4.3 Change of Ground State

However, a difference becomes visible when we look closer at the individual bands (figure 16b.), there seems to be a regime change between $U/t = 30$ and $U/t = 40$, which can be seen by the bright excitations not occupying the same energies above $U/t = 30$ as for lower values of U/t. To get a better idea of where this change is coming from and what is causing it we look at the change of ground state and excited state energies with respect to changes in U/t (figure 17a.). Looking closer at the two lowest energy states (figure 17b.), we can see a definite crossing of ground states from a total angular momentum of $2\pi/3$ to one of $\pi/3$. It is this change which accounts for the regime change that we observe in the optical emission spectrum.

4.4.4 S=1/2 Case

Next we look at the total spin 1/2 case which is the actual ground state of the five electron system for finite U. This case also allows the creation of Hubbard bands, with an additional band to account for the added minority spin, as we can see in figure 18a.

4.4.5 Change of Ground State

As in the 3/2 case, we notice a change of regime, and so we take a closer look at the Hubbard bands (figure 18b.), the ground, and the excited state energies (figure 19a.). We observe that this optical change results from a crossing of the degenerate ground state with a non degenerate excited state (figure 19b.). This

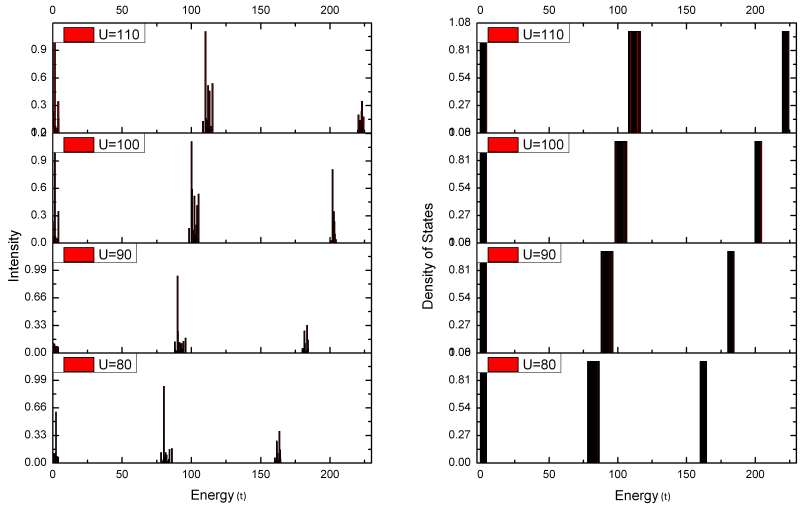

a)

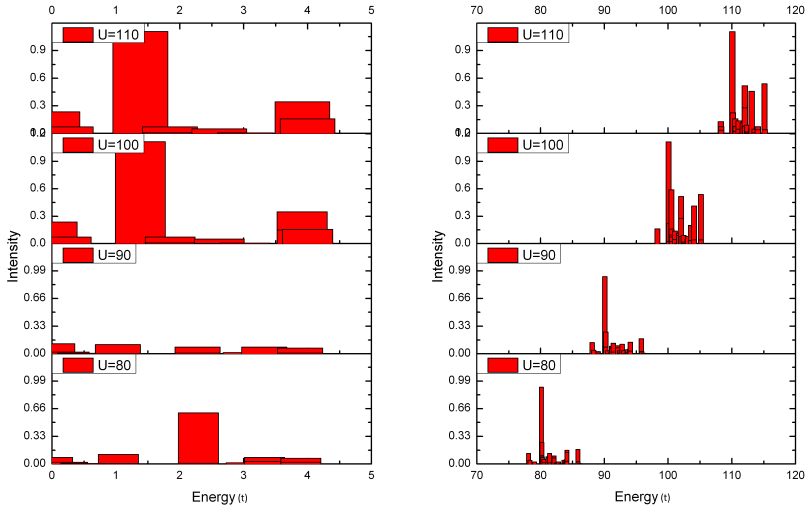

b)

Figure 18: Absorption spectrum of charged ABR, $S = 1/2$, with V = 0: a) Absorption spectrum for values of U ranging from 80 to 110, we have the intensities and the energy levels side by side to show which are bright. b) Magnified look at two of the lowest Hubbard bands.

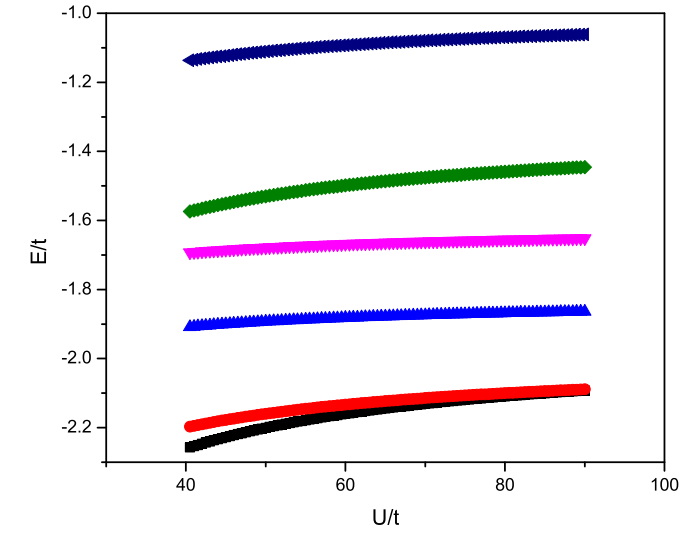

a)

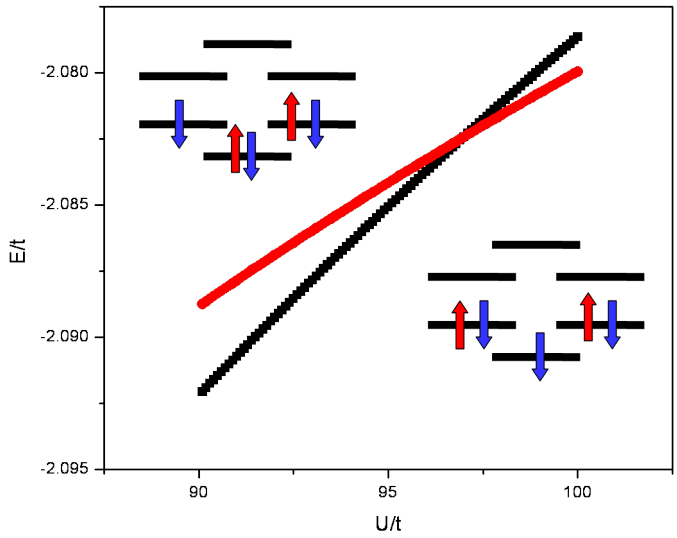

b)

Figure 19: Five electron spin 1/2 case, with V = 0: a) Ground state and first five excited energy levels changing with respect to U/t. b) Magnified portion of U/t = 90 to 100 to show the crossing of an excited state with the ground state, the dominant configurations for the states are shown, with the original ground state on the left, and the new one on the right.

crossing also results in a change of total angular momentum from $\pi/3$ to 0.

5 Summary

To summarize, this thesis has presented a theory of the electronic and optical properties of an ABR with up to six electrons. This structure was described by the extended Hubbard model and was solved using exact diagonalization in real and Fourier space using the configuration interaction method. We determined that the ground states, the dominant configurations of the electrons at lowest energy, for the three and the five electron case can be tuned both between their excited states in the same total spin, and even the total spin ordering of the system can be changed. In the charged case, we see an emergence of an artificial gauge field when minority carriers were present. The total spin of the electron configurations were resolved by $\hat{S}^2$ constructed bases, through the use of spin currents, as well as numerically. The optical spectra of the charge neutral and charged cases were explored and examined, both analytically in a simplified case as well as numerically. For the $N_e = 5$ cases we see how the ground states change for high interactions through the change of the optical spectra.

References

[1] P. Hawrylak and M. Korkusinski, "Electronic Properties of Self-Assembled Quantum Dots", in: P.Michler(Ed.), "Single Quantum Dots, Fundamentals, Applications and New Concepts"(Springer, Berlin, 2003).

[2] L. Jacak, P. Hawrylak, A. Wójs, "Quantum Dots"(Springer, 1998).

[3] M. Ciorga, A. S. Sachrajda, P. Hawrylak, C. Gould, P. Zawadzki, S. Jullian, Y. Feng, Z. Wasilewski, Phys. Rev. B **61**, R16315 (2000).

[4] S. Tarucha, D. G. Austing, T. Honda, R. J. van der Hage, L. P. Kouwenhoven, Phys. Rev. Lett. **77**, 3613 (1996).

[5] P. Hawrylak, C. Gould, A. Sachrajda, Y. Feng, Z. Wasilewski, Phys. Rev. B **59**, 2801 (1999).

[6] A. W. Holleitner, R. H. Blick, A. K. Hüttel, K. Eberl, J. P. Kotthaus, Science 297, **70** (2002).

[7] M. Pioro-Ladriere, R. Abolfath, P. Zawadzki, J. Lapointe, S. Studenikin, A. S. Sachrajda, P. Hawrylak, Phys. Rev. B **72**, 125307 (2005).

[8] F. H. Koppens, J. A. Folk, J. M. Elzerman, R. Hanson, L. H. W. van Beveren, I. T. Vink, H. P. Tranitz, W. Wegscheider, L. P. Kouwenhoven, L. M. K. Vandersypen, Science **309**, 1346 (2005).

[9] J. R. Petta, A. C. Johnson, J. M. Taylor, E. A. Laird, A. Yacoby, M. D. Lukin, C. M. Marcus, M. P. Hanson, A. C. Gossard, Science **309**, 2180 (2005).

[10] T. Hatano, M. Stopa, S. Tarucha, Science **309**, 268 (2005).

[11] J. M. Elzerman, R. Hanson, L. H. W. van Beveren, B. Witkamp, L. M. K. Vandersypen, L. P. Kouwenhoven, Nature **430**, 431 (2004).

[12] L. Gaudreau, S. A. Studenikin, A. S. Sachrajda, P. Zawadzki, A. Kam, J. Lapointe, M. Korkusinski, P. Hawrylak, Phys. Rev. Lett. **97**, 036807 (2006).

[13] D. Schröer, A. D. Greentree, L. Gaudreau, K. Eberl, L. C. L. Hollenberg, J. P. Kotthaus, S. Ludwig, Phys. Rev. B **76**, 075306 (2007).

[14] T. Ihn, M. Sigrist, K. Ensslin, W. Wegscheider, M. Reinwald, New J. of Phys. **9**, 111 (2007).

[15] M. C. Rogge, R. J. Haug, Phys, Rev. B **78**, 153310 (2008).

[16] E. A. Laird, J. M. Taylor, D. P. DiVincenzo, C. M. Marcus, M. P. Hanson, A. C. Gossard, Phys. Rev. B **82**, 075403 (2010).

[17] S. Amaha, T. Hatano, H. Tamura, S. Teraoka, T. Kubo, Y. Tokura, D. G. Austing, S. Tarucha, Phys. Rev. B **85**, 081301 (2012).

[18] C. -Y. Hsieh, Y. -P. Shim, M. Korkusinski, P. Hawrylak, Rep. Prog. Phys. **75**, 114501 (2012).

[19] P. Hawrylak, M. Korkusinski, Solid State Commun. **136**, 508 (2005).

[20] M. Korkusinski, I. Puerto-Gimenez, P. Hawrylak, L. Gaudreau, S. A. Studenikin, A. S. Sachrajda, Phys. Rev. B **75**, 115301 (2007).

[21] I. Puerto-Gimenez, M. Korkusinski, P. Hawrylak, Phys. Rev. B **76**, 075336 (2007).

[22] F. Delgado, Y. P. Shim, M. Korkusinski, L. Gaudreau, S. Studenikin, A. S. Sachrajda, P. Hawrylak, Phys. Rev. Lett. **101**, 226810 (2008).

[23] I. Puerto-Gimenez, C.-Y. Hsieh, M. Korkusinski, P. Hawrylak, Phys. Rev. B **79**, 205311 (2009).

[24] J. A. Brum, P. Hawrylak, Superlattices Microstruct. **22**, 431 (1997).

[25] A. M. Lobos, A. A. Aligia, Phys. Rev. Lett. **100**, 016803 (2008).

[26] Y. Nisikawa, A. Oguri, Phys. Rev. B **73**, 125108 (2006).

[27] A. Sharma, P. Hawrylak, Phys. Rev. B **83**, 125311 (2011).

[28] V. W. Scarola, S. Das Sarma, Phys. Rev. A **71**, 032340 (2005).

[29] A. Mizel, D. A. Lidar, Phys. Rev. B **70**, 115310 (2004).

[30] I. Ozfidan, A. Trojnar, M. Korkusinski, P. Hawrylak, Solid State Communications vol. **172**, 15-19 (2013).

[31] M. D. Shulman, O.E. Dial, S. P. Harvey, H. Bluhm, V. Umansky, A. Yacoby, Science **336**, 202 (2012).

[32] R. Thalineau, S. Hermalin, A. D. Wieck, C. Bäuerle, L. Saminadayar, T. Meunier, Appl. Phys. Lett. **101**, 103102 (2012).

[33] C. Blömers, T. Rieger, P. Zellekens, F. Haas, M. I. Lepsa, H. Hardtdegen, Ö. Gül, N. Demarina, D. Grützmacher, H. Lüth, T. Schäpers, Nanotechnology **24**, 035203 (2013).

[34] S. Albert, A. Bengoechea-Encabo, M. Sabido-Siller, M. Müller, G. Schmidt, S. Metzner, P. Veit, F. Bertram, M. A. Sánchez-García, J. Christen, E. Calleja, J. of Crystal Growth **392** (2014).

[35] P. J. Poole, D. Dalacu, X. Wu, J. Lapointe, K. Mnaymneh, Nanotechnology **23**, 385205 (2012)

[36] A. Ballester, J. Planelles, A. Bertoni, J. Appl. Phys. **112**, 104317 (2012).

[37] Cooper, David L.; Gerratt, Joseph; Raimondi, Mario, Nature **323** 6090, (1986)

[38] L. Pauling, Nature **325** 6103, (1987)

[39] Messmer, Richard P.; Schultz, Peter A., Nature **329** 6139, (1987)

[40] Harcourt, Richard D., Nature **329** 6139, (1987)

[41] K. McMichael, Organic Chemistry, Washington State University, http://chemistry2.csudh.edu/rpendarvis/BenzStr.html, (2001)

[42] M. Polini, F. Guinea, M. Lewenstein, H. C. Manoharan, V. Pellegrini, Nature Nanotechnology **8**, 625-633 (2013).

[43] M. Korkusinski, Phd Thesis (2004).

[44] W. J. Caspers, P. L. Iske, Physica A, 1989, vol. 157, issue **2**, pages 1033-1041.

[45] I. Ozfidan, M. Vladisavljevic, M. Korkusinski, P. Hawrylak, unpublished (2014).

[46] I. Ozfidan, M. Korkusinski, A. Devrim Güclü, J. A. McGuire, P. Hawrylak, Phys. Rev. B **89**, 085310 (2014).

[47] P. Potasz, A. D. Güclü, P. Hawrylak, Phys. Rev. B **82**, 075425 (2010)